Commun. Theor. Phys. **77** (2025) 065001 (20pp)
https://doi.org/10.1088/1572-9494/ada495
CSTR: 32041.14.CTP.ada495

A study of feedback loop mechanisms regulating calcium, IP_3 and dopamine in neurons

Anand Pawar* **and Kamal Raj Pardasani**

Department of Mathematics, Bioinformatics and Computer Applications, Maulana Azad National Institute of Technology, Bhopal-462003, Madhya Pradesh, India

E-mail: pawar.anand1902@gmail.com and kamalrajp@rediffmail.com

Received 15 August 2024, revised 1 January 2025
Accepted for publication 2 January 2025
Published 19 March 2025

Abstract

The present work primarily aims to explore the neuronal calcium (Ca^{2+}), IP_3, and dopamine (DA) signaling systems through a feedback loop model. To date, there has been no exploration of this feedback model in fractional-order dynamical systems. This feedback loop model incorporates several crucial mechanisms like the buffering process, IP_3-receptor, ryanodine receptor, plasma membrane Ca^{2+} ATPase and sarcoplasmic/endoplasmic reticulum calcium ATPase (SERCA) pump, leak, sodium-calcium exchanger, voltage-gated Ca^{2+} channel, Orai channels, DA-dependent IP_3 synthesis, and others. By incorporating these mechanisms, the model aims to provide a more comprehensive and realistic understanding of the system under investigation. The present model incorporates fractional-order dynamics along both spatial and temporal dimensions to examine the impacts of superdiffusion and memory showing Brownian motion of Ca^{2+}, IP_3, and DA signaling molecules. The bidirectional feedback between calcium and IP_3 signaling systems, unidirectional feedback between calcium and dopamine signaling systems, and unidirectional feedback between IP_3 and dopamine signaling systems have been incorporated into the present model. These feedback loops establish interactions among calcium, IP_3, and dopamine signaling systems within neuronal cells. The numerical findings were obtained by using the Crank–Nicholson method with the Grunwald technique for fractional space derivatives and the L_1 method for fractional time derivatives in conjunction with the Gauss–Seidel Iterations. This research specifically investigates the implications of cell memory as well as superdiffusion on Ca^{2+}, IP_3, and DA dynamics in neuronal cells, which are interactive nonlinear systems. The superdiffusion process results in a reduction in Ca^{2+}, IP_3, and DA concentrations, while cellular memory leads to an increase in ion and molecule concentrations in neuronal cells during the initial time. The disruption of any given process can lead to imbalances in calcium, IP_3, and DA systems, hence contributing to neurotoxicity and cellular demise.

Keywords: feedback loop among Ca^{2+}, IP_3 and dopamine systems, reaction-diffusion equations, fractional-order dynamics, superdiffusion, cell memory

(Some figures may appear in colour only in the online journal)

Introduction

An assortment of cellular processes, including but not limited to diffusion, buffering, influx, and outflux mechanisms, play a role in the complex and versatile bioenergetic systems that facilitate chemical signaling. This process is observed in various cells like neurons and is mediated by calcium, IP_3, and dopamine signaling molecules. Neuronal cell calcium signaling is essential for the regulation of numerous cellular processes. Neuronal disorders may manifest due to any disruption in the calcium signaling pathway. Alzheimer's disease (AD) has been associated with alterations in calcium

* Author to whom any correspondence should be addressed.

buffering [1], hyperregulation of the sarcoplasmic/endoplasmic reticulum calcium ATPase (SERCA) pump and leak activities [2], and heightened sensitivity of calcium release channels [3]. Nevertheless, under realistic circumstances, calcium regulation depends on the interplay of additional signaling systems, including IP_3 and DA, which occur within neuronal cells. The IP_3 molecule facilitates the increase of cytosolic Ca^{2+} levels by discharging Ca^{2+} ions from the endoplasmic reticulum (ER) to the cytosol; it operates as a secondary messenger. Multiple cellular processes, including cell proliferation, fertilization, cell transformation, and muscular contraction, are intricately regulated by this process. Dopamine is a neurochemical messenger that has a significant concentration inside the midbrain region of the central nervous system [4]. Dopamine is a potentially harmful chemical that has been associated with the onset of neurodegenerative conditions like Parkinson's disease (PD) [5]. Dopamine is influenced by a wide range of metabolites, many biological constituents, and a diverse array of environmental and genetic influences in neuronal cells. The mathematical investigation of DA signaling and its potential relevance to Parkinson's illness has been reported in cells [6].

The cell utilizes two separate sources of calcium ions to generate signals: the discharge of Ca^{2+} ions from internal cellular compartments and the Ca^{2+} inflow across the plasma membrane. Both the processes of releasing and entering Ca^{2+} can produce highly localized Ca^{2+} signals, which are regarded as essential events in Ca^{2+} signaling [7]. The ryanodine receptor (RyR) and IP_3-receptor (IP_3R) are distinct Ca^{2+}-releasing channels positioned within the ER membrane [8]. The calcium buffering mechanism involves the use of both stationary and mobile buffers, which significantly affects the movement of calcium ions in cellular settings [9]. A calcium buffer was used to induce a quantifiable decrease in the alteration of free calcium levels following a transient infusion of calcium [10]. Recent studies examined the phenomenon of calcium signaling and its modulation in many types of human cells, such as neurons [11–16], astrocytes [17, 18], acinar [19, 20], myocyte [21, 22], Oocyte [23–27], fibroblast cells [28, 29], hepatocyte [30–32] and T-lymphocyte [33]. An investigation has been carried out on the process of diffusion of calcium ions within neuron cells using the excess buffer approximation as a theoretical framework. This framework includes the impact of sodium (Na^+) ions on the movement of calcium, while also including different sources of Ca^{2+} and Na^+ in neurons [34]. The study investigated calcium diffusion using a two-dimensional model, taking into consideration several elements such as buffer, diffusion coefficients, and flux, to accurately assess their impacts [35]. The external environment has a crucial impact on the regulation of cytosolic Ca^{2+} levels in neuronal cells by governing the inflow and outflow of Ca^{2+} ions through the plasma membrane [36].

There has been a lack of extensive research on the connections between calcium and IP_3 systems in various types of human cells, both in experimental and theoretical settings. The findings obtained by analyzing interconnected signaling systems such as Ca^{2+} and IP_3 reveal significant disparities when compared to those obtained from examining separate signaling systems such as Ca^{2+} in neuronal cells. The structure and functioning of IP_3-mediated Ca^{2+} signaling have a substantial impact on the control of brain activity [37]. Observations have been made about the link between fluctuations and chaotic dynamics in Ca^{2+} signaling, as well as the coexistence of dynamic calcium and constant IP_3 within neural cells [38]. A study has reported a nine-variable kinetic model that accurately describes the behavior of the IP_3R channel by using quantitative measurements of Ca^{2+} ions activation and inhibition of the IP_3-receptor situated in the ER [39]. The nine-variable IP_3R model has been analyzed and simplified, resulting in a two-variable system [40]. Measuring the transportation coefficient of IP_3 and Ca^{2+} is important for determining the extent of messenger action from a localized source of calcium and IP_3 inside cellular contexts [41]. The interplay between the concentration of calcium ions and inositol trisphosphate results in the creation of a state of bistability. This is achieved by a feedback process where Ca^{2+} concentration influences the formation of IP_3, and the discharge of calcium ions is regulated by both calcium ions and IP_3 [42]. The investigations undertaken on the calcium and IP_3 signaling systems have been the subject of recent reports. These investigations have revealed their role in regulating many mechanisms in different cell types, such as neurons [43, 44], hepatocytes [45], β-cell [46], fibroblast cells [47, 48], T-lymphocyte [49], and others. Prior studies have examined the exploration of the interrelated spatial and temporal impacts of Ca^{2+} and IP_3 mechanics, together with their contributions to the generation of nitric oxide [50] and β-amyloid [51], and the release of ATP [52] in neuronal cells.

Several calcium-activated channels, including voltage-gated Ca^{2+} channels (VGCC) [53], are involved in controlling the distinct functions of dopamine neuron cells. PD is identified by the deterioration of dopaminergic neurons, which is influenced by high levels of calcium, dopamine, and α-synuclein [54]. The function of the Calbindin-D_{28K} buffer in safeguarding dopaminergic neuronal cells against the pathological process that causes PD was elucidated in the literature [55]. The increase in Ca^{2+} ion concentration can be attributed to the presence of a small quantity of calbindin-D_{28k}, which is both indicative and characteristic of Parkinson's disease [56]. Several mechanisms such as source influx, buffering, ryanodine receptor activity, and other factors have been identified as contributors to the high levels of calcium and dopamine that eventually result in the death of dopaminergic neurons [57].

Utilizing fractional calculus in the analysis of biological systems provides a more profound understanding of the intricate mechanisms exhibited by different cells and tissues [58]. Various numerical approaches such as the Grunwald approximation are employed to solve the fractional derivatives along spatial dimensions [59]. The fractional model is utilized to elucidate memory phenomena across several disciplines, encompassing mechanics, biology, and psychology [60]. Cell memory is commonly linked to fractional-order systems, and cells acquire learning through their encounters with disease-related circumstances [61]. A notable finding reported in the

literature is that the memory trace begins to emerge when the fractional order increases from 0 to 1 and entirely vanishes when the order reaches 1 [62]. The Ca^{2+} dynamics within neurons are characterized using a fractional reaction-diffusion framework that incorporates the presence of calcium-binding proteins [63]. Cell memory is found to have a notable influence on protein and VGCC. Cellular memory reduces the influx of calcium ions with elevation, leading to improved outcomes in estimating the Ca^{2+} flow during pathological conditions [64]. Superdiffusion is a rare occurrence that can be observed in several situations, such as biological systems and the motion of organic molecules [65]. The augmentation of the diffusion mechanism is noted when the fractional derivatives are employed as replacements for the second-order derivatives inside the diffusion framework. The phenomenon characterized by an enhanced rate of diffusion is commonly referred to as superdiffusion [66]. The studies on the effects of memory and superdiffusion on the interacting signaling of Ca^{2+} and IP_3 [67], Ca^{2+} and β-amyloid [68], Ca^{2+} and NO [69], Ca^{2+} and DA [70], and Ca^{2+}, IP_3, and β-amyloid [71] in neurons have been analyzed with numerical findings. These investigations have revealed a significant discrepancy in results when comparing systems with fractional-order dynamics to those with integer-order dynamics.

The existing integer-order models of Ca^{2+}, IP_3, and DA systems in the literature exhibit mutual interactions among these signaling systems in neuronal cells, providing significant insights into many biological functions within neuronal cells. However, there is no documented research on the interaction among Ca^{2+}, IP_3, and DA in nonlinear fractional-order dynamics, which illustrates the impacts of superdiffusion and cellular memory with Brownian motion (BM) in neuronal cells. The principal advantage of examining the space-time fractional reaction-diffusion equation compared to the classical diffusion equation is its global behavior. The integer-order differential equation acts as a local operator, while the fractional (non-integer) order differential equation performs as a non-local operator. Estimating the spatial and temporal profiles of Ca^{2+}, IP_3, and DA in neurons in any certain state depends not only on the current profiles of these molecules but also on all prior profiles of Ca^{2+}, IP_3, and DA. The dynamics of the fractional reaction-diffusion equation facilitate the calculation of precise concentration profiles for Ca^{2+}, IP_3, and DA clarifying the complex mechanisms involved in the nervous system. Therefore, a fractional-order reaction-diffusion model of interacting Ca^{2+}, IP_3, and DA has been developed in neurons. This paper presents the framework of a feedback loop model with fractional order to accurately represent neuronal calcium, IP_3, and DA signaling, which interact with nonlinear dynamics. The computational method utilized in this study involves the implementation of the Crank–Nicholson (CN) scheme in conjunction with the Grunwald technique for spatial dimensions. Additionally, the L1 scheme is applied for temporal dimensions, and Gauss–Seidel Iterations (GSI) is used for the solution process. The feedback loop framework incorporates the reciprocal relationship between Ca^{2+} and IP_3, the one-way relationship between Ca^{2+} and DA, and the one-way relationship between DA and IP_3, along with various crucial such as VGCC, plasma membrane Ca^{2+} ATPase (PMCA) channel, sodium–calcium exchanger (NCX), buffer, STIM-Orai channel, RyR, IP_3R, etc in neuronal cells. This study investigates the impact of various significant processes such as superdiffusion and memory characterized by BM on the interacting calcium, IP_3, and DA signaling in neuronal cells providing novel insights into these impacts.

Mathematical formulation

The existing integer-order Ca^{2+} model proposed by Wagner *et al* [42] has been extended to fractional order along both spatial and temporal dimensions. This extended model also incorporates the EGTA buffer, VGCC, STIM-Orai, PMCA, NCX, and RyR into the fractional-order Ca^{2+} framework and can be depicted as follows:

$$\begin{aligned}\frac{\partial^{U1}[Ca^{2+}]}{\partial t^{U1}} &= D_{Ca}\frac{\partial^{V1}[Ca^{2+}]}{\partial x^{V1}} \\ &+ \left(\frac{J_{IPR} + J_{LEAK} + J_{RyR} - J_{SERCA}}{F_C}\right) \\ &- K^{+}[B]_{\infty}([Ca^{2+}] - [Ca^{2+}]_{\infty}) \\ &+ J_{VGCC} - J_{PMCA}. \end{aligned} \tag{1}$$

In this context, $0 < U_1 \leqslant 1$, $1 < V_1 \leqslant 2$. The parameters $[B]_{\infty}$ and $[Ca^{2+}]_{\infty}$ denote the equilibrium concentrations of buffer and Ca^{2+} ions in neuronal cells, respectively. The variables t and x are employed to denote the temporal and spatial dimensions, respectively. The diffusion coefficient of calcium ions is denoted as D_{Ca}, while the rate at which calcium ions associate with buffers is represented by K^{+}.

The flux of IP_3-receptor (J_{IPR}) denotes the process by which calcium is released from ER to the cytosol of neuronal cells in response to IP_3 stimulation as follows [42],

$$J_{IPR} = V_{IPR}m^3h^3([Ca^{2+}]_{ER} - [Ca^{2+}]). \tag{2}$$

The following are the mathematical depiction of the variables m and h [40],

$$m = \left(\frac{[IP_3]}{[IP_3] + K_{IP3}}\right)\left(\frac{[Ca^{2+}]}{[Ca^{2+}] + K_{Ac}}\right), \tag{3}$$

$$h = \frac{K_{inh}}{K_{Inh} + [Ca^{2+}]}. \tag{4}$$

The parameters K_{IP3}, K_{Ac}, and K_{inh} stand for the dissociation constants associated with the binding location of inositol trisphosphate and the activation and inhibition of Ca^{2+} in neuronal cells.

The SERCA pump flux (J_{SERCA}) depicts the SERCA pump activity, which causes the translocation of cytosolic calcium ions from neuronal cells to the ER. The mathematical representation for the J_{SERCA} is as follows [42],

$$J_{SERCA} = V_{SERCA}\left(\frac{[Ca^{2+}]^2}{[Ca^{2+}]^2 + K_{SERCA}^2}\right). \tag{5}$$

In this context, the variables V_{SERCA} and K_{SERCA} are employed to denote the rate at which flux occurs and the

constant that characterizes the Michaelis–Menten kinetics, respectively, for the SERCA pump.

The leak flux (J_{Leak}) exhibits the leakage event, in which the gradual diffusion of Ca^{2+} ions from the ER membrane to the cytoplasm, occurs in the following manner [42],

$$J_{\text{LEAK}} = V_{\text{LEAK}}([Ca^{2+}]_{\text{ER}} - [Ca^{2+}]), \tag{6}$$

where the variable V_{LEAK} is employed to denote the flux rate associated with the leak mechanism.

The RyR flux (J_{RyR}) exhibits the activities of the RyR, which mediates Ca^{2+} from the ER to the cytosol, in the following manner.

$$J_{\text{RyR}} = P_0 V_{\text{RyR}}([Ca^{2+}]_{\text{ER}} - [Ca^{2+}]). \tag{7}$$

In this context, the variable V_{RyR} is employed to denote the flux rate constant associated with the RyR, while P_0 represents the open probability of the RyR that ranges from 0 to 1.

The current equation proposed by Goldmann–Hodgkin–Kartz is utilized to simulate the flow of voltage-gated calcium channels (J_{VGCC}) as follows,

$$I_{\text{Ca}} = \frac{P_{\text{Ca}} Z_{\text{Ca}}^2 F^2 V_m}{RT} \frac{[Ca^{2+}]_i - [Ca^{2+}]_0 \exp\left(-Z_{\text{Ca}} \frac{FV_m}{RT}\right)}{1 - \exp\left(-Z_{\text{Ca}} \frac{FV_m}{RT}\right)}. \tag{8}$$

Here, equation (8) incorporates the extracellular concentration of calcium ions ($[Ca^{2+}]_0$), the intracellular concentration of calcium ions ($[Ca^{2+}]_i$), the permeability of calcium ions (P_{Ca}), valency of calcium ions (Z_{Ca}), membrane potential (V_m), Faraday's parameter (F), real gas constant (R), and absolute temperature (T). The mathematical representation for converting equation (8) into the unit of molar/second is depicted in the following manner,

$$J_{\text{VGCC}} = -\frac{I_{\text{Ca}}}{Z_{\text{Ca}} F V_{\text{cytosol}}}. \tag{9}$$

In neural cells, The NCX enables the transfer of a single calcium ion in exchange for three Na^+ ions. The following is the mathematical representation for the NCX,

$$J_{\text{NCX}} = \text{Ca}_0 \left(\frac{\text{Na}_i}{\text{Na}_0}\right)^3 \exp\left(\frac{FV_m}{RT}\right), \tag{10}$$

where, the variables Na_i and Na_0 represent the respective levels of intracellular and extracellular Na^+ ions.

The PMCA pump flux (J_{PMCA}) exhibits the activities of the PMCA pump, which facilitates the removal of cytosolic calcium from the intracellular environment to the extracellular space in the following manner,

$$J_{\text{PMCA}} = V_{\text{PMCA}} \left(\frac{[Ca^{2+}]^2}{[Ca^{2+}]^2 + K_{\text{PMCA}}^2}\right). \tag{11}$$

In this context, the parameters V_{PMCA} and K_{PMCA} are employed to depict the flux rate constant and the dissociation pump rate for the PMCA, respectively.

The Orai channel (J_{Orai}) flux exhibits the Orai channel activities, which facilitates the transfer of Ca^{2+} from the external environment to the cytosol in the following manner,

$$J_{\text{Orai}} = \phi \frac{I_{\text{Orai}}}{A_0 z F}. \tag{12}$$

Here, ϕ represents the open probability, whereas A_0 and I_{Orai} respectively denote the area and current of the Orai channel.

The equation representing the Ca^{2+} content in the ER ($[Ca^{2+}]_{\text{ER}}$) can be depicted in the following manner [42]:

$$[Ca^{2+}]_{\text{ER}} = \left(\frac{[Ca^{2+}]_T - F_C[Ca^{2+}]_C}{F_E}\right). \tag{13}$$

The existing integer-order IP_3 framework proposed by Wagner *et al* [42] has been extended to fractional order along both spatial and temporal dimensions. This extended model also incorporates the Ca^{2+}-dependent and DA-dependent flux of IP_3 production into the fractional-order IP_3 model and can be expressed as follows:

$$\frac{\partial^{U_2}[\text{IP}_3]}{\partial t^{U_2}} = D_i \frac{\partial^{V_2}[\text{IP}_3]}{\partial x^{V_2}} + \frac{J_{\text{production}} - \lambda(J_{\text{phosphatase}} + J_{\text{kinase}})}{F_C} + J_{\text{DA}}, \tag{14}$$

where $0 < U_2 \leqslant 1$, $1 < V_2 \leqslant 2$. The IP_3 diffusion coefficient is exhibited by D_i. The term $J_{\text{production}}$ is used to symbolize the flux of calcium-dependent inositol trisphosphate generation in as follows [42],

$$J_{\text{production}} = V_{\text{production}} \left(\frac{[Ca^{2+}]^2}{[Ca^{2+}]^2 + K_{\text{production}}^2}\right). \tag{15}$$

Here, the IP_3 generation rate and the Michaelis parameter concerning the activation of Ca^{2+} are denoted as $V_{\text{Production}}$ and $K_{\text{Production}}$, respectively. The mathematical expressions for the flux of degradation of inositol trisphosphate by J_{Kinase} [72] and $J_{\text{phosphatase}}$ [73] are depicted as follows,

$$J_{\text{kinase}} = (1 - \theta) V_a \left(\frac{[\text{IP}_3]}{[\text{IP}_3] + 2.5}\right) + \theta V_b \left(\frac{[\text{IP}_3]}{[\text{IP}_3] + 0.5}\right), \tag{16}$$

$$J_{\text{phosphatase}} = V_{\text{ph}} \left(\frac{[\text{IP}_3]}{[\text{IP}_3] + 30}\right), \tag{17}$$

$$\theta = \left(\frac{[Ca^{2+}]}{[Ca^{2+}] + 0.39}\right). \tag{18}$$

Here, the parameters associated with low and high concentrations of calcium ions (3-kinase) are denoted as V_a and V_b, respectively. Additionally, V_{ph} represents the maximal rate constant of the phosphatase. The flexible parameter λ depicts the elimination rate of IP_3 [42].

The process of IP_3 synthesis through the activation of D_1-receptor and its reliance on dopamine can be represented by the following mathematical expressions,

$$J_{\text{DA}} = V_{\text{DA}} \frac{[\text{DA}]^\beta}{[\text{DA}]^\beta + \left(K_{\text{DA}} + K_P \frac{[Ca^{2+}]}{[Ca^{2+}] + K_{P1}}\right)^\beta}, \tag{19}$$

where the maximum formation rate of IP_3 by phospholipase C (PLC) due to D_1-receptor activation is denoted as V_{DA}. The binding strength of DA to the receptor is represented by the affinity constant, K_{DA}.

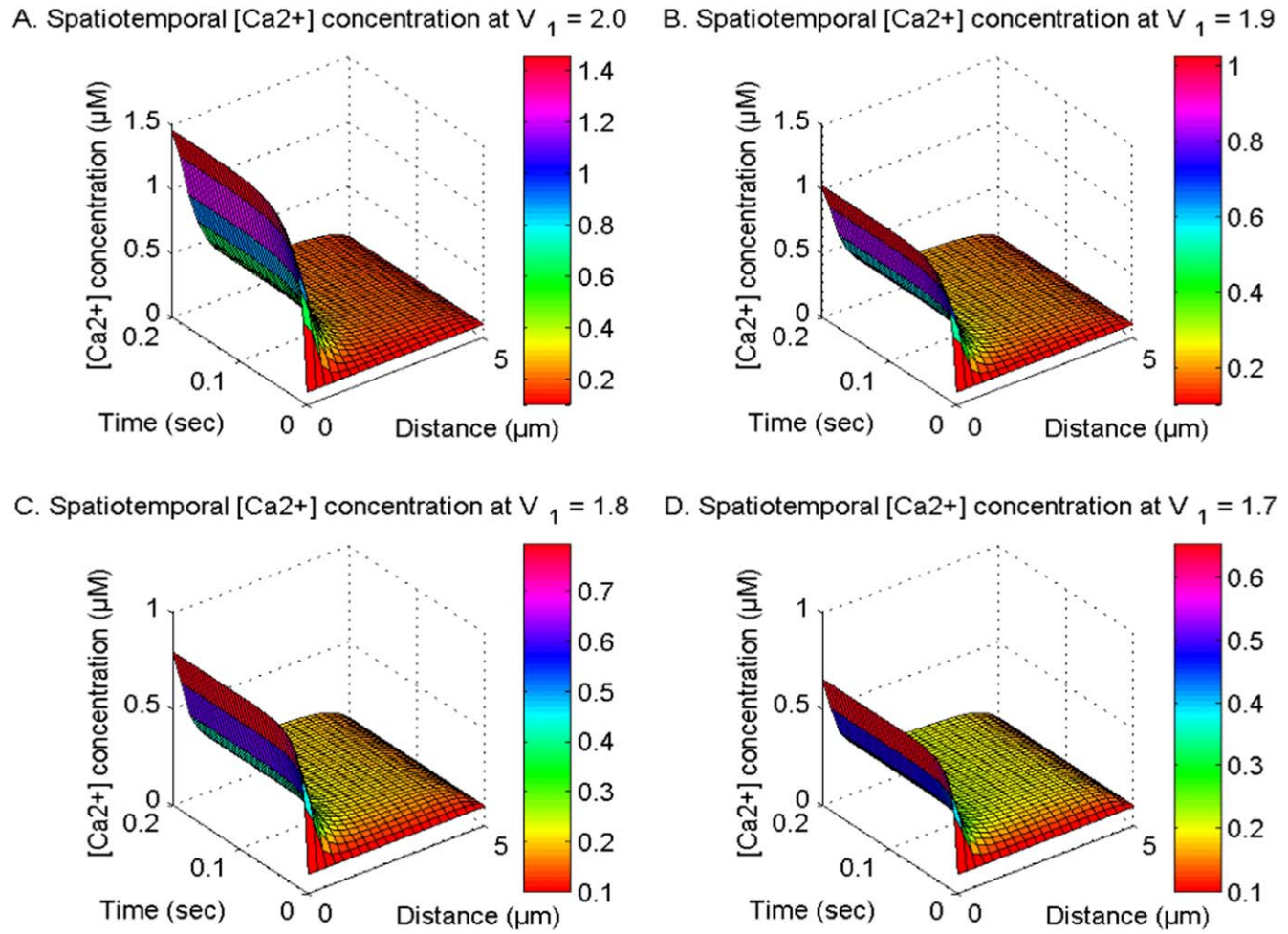

Figure 1. The spatiotemporal Ca^{2+} distribution at U_1, U_2 and $U_3 = 1.0$ and V_2 $V_3 = 2.0$ with NCX, PMCA, VGCC and Orai channel for $V_1 = 2$, 1.9, 1.8 and 1.7.

The existing integer-order DA model proposed by Tello-Bravo [74] has been extended to fractional order along both spatial and temporal dimensions. This extended model also incorporates the Ca^{2+}-dependent DA production into the fractional-order DA model and can be expressed as follows:

$$\frac{\partial^{U_3}[\mathrm{DA}]}{\partial t^{U_3}} = D_{\mathrm{DA}} \frac{\partial^{V_3}[\mathrm{DA}]}{\partial x^{V_3}} + \left(J_{\mathrm{release}} + [\mathrm{DA}]_P f - \frac{V_{\max}[\mathrm{DA}]}{([\mathrm{DA}] + K_{\mathrm{m}})} \right). \quad (20)$$

Here, $0 < U_3 \leqslant 1$, $1 < V_3 \leqslant 2$. The parameter D_{DA} represents the DA diffusion coefficient. Equation (20) incorporates the dopamine release per electrical stimulus pulse (DA_P), stimulus frequency (f), Michaelis parameter (K_{m}) and DA uptake rate ($V_{\max}$). The formulation of $[Ca^{2+}]$-dependent dopamine release is presented as follows [74],

$$J_{\mathrm{release}} = \psi . n_{\mathrm{RRP}} . P_{\mathrm{rel}} \left(\frac{[Ca^{2+}]^4}{[Ca^{2+}]^4 + K_{\mathrm{rel}}^4} \right), \quad (21)$$

where the term J_{release} represents the flux of DA release. Equation (21) incorporates the average release flux (Ψ), high release probability (P_{rel}) and Ca^{2+} sensitivity (K_{rel}) in neuronal cells.

Initial conditions

The initial concentration for the Ca^{2+} [75], inositol trisphosphate [76], and dopamine [77] are shown as follows,

$$[Ca^{2+}]_{t=0} = 0.1\ \mu\mathrm{M}. \quad (22)$$

$$[\mathrm{IP_3}]_{t=0} = 0.16\ \mu\mathrm{M}. \quad (23)$$

$$[\mathrm{DA}]_{t=0} = 0\ \mu\mathrm{M}. \quad (24)$$

Boundary conditions

The boundary circumstances for Ca^{2+} as follows [75],

$$\lim_{x \to 0} \left(-D_{\mathrm{Ca}} \frac{\partial [Ca^{2+}]}{\partial x} \right) = \sigma - J_{\mathrm{NCX}} + J_{\mathrm{Orai}}, \quad (25)$$

The symbol σ shows the Ca^{2+} influx.

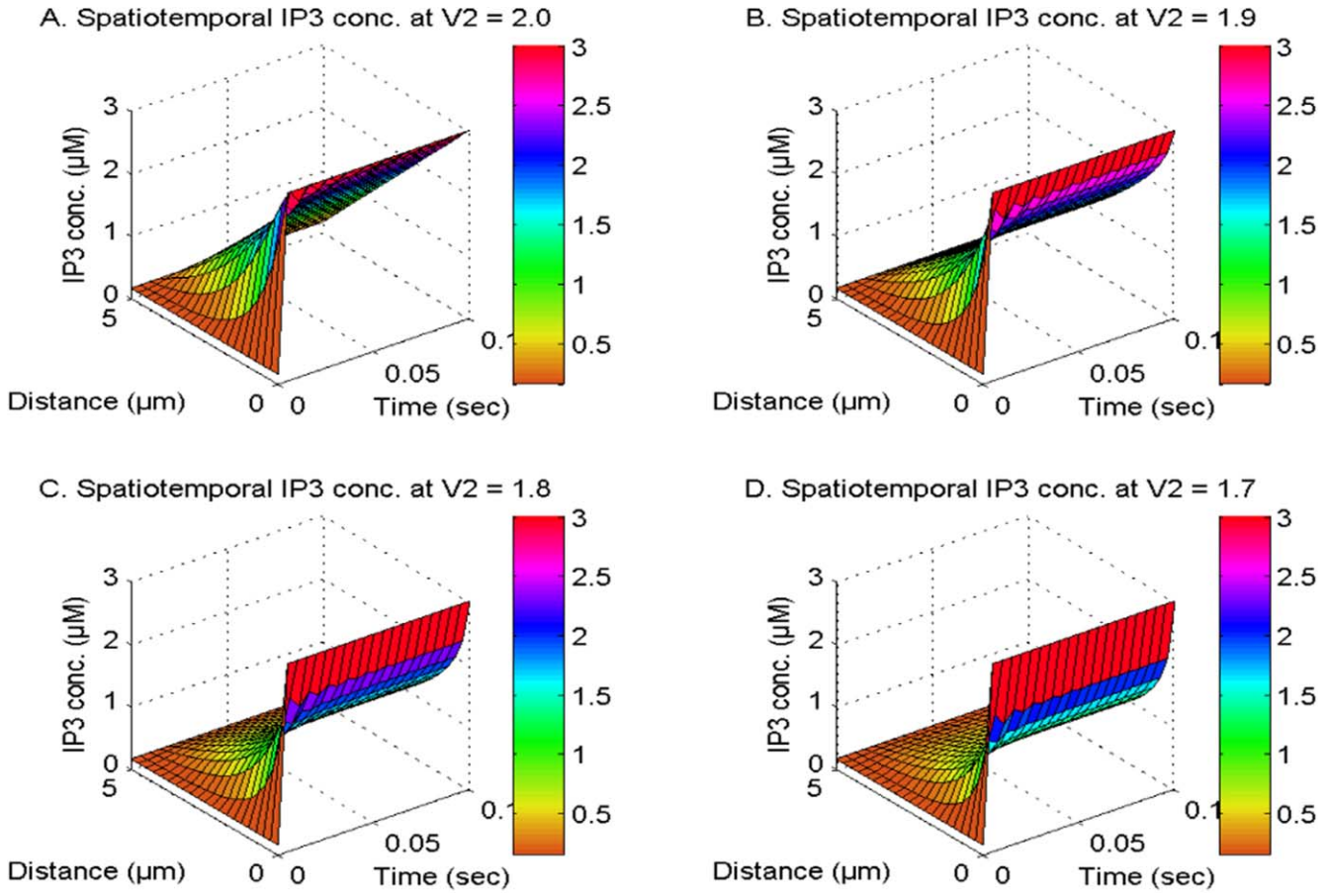

Figure 2. The spatiotemporal IP3 distribution at U_1, U_2 and $U_3 = 1.0$ and V_1 and $V_3 = 2.0$ with NCX, PMCA, VGCC and Orai channel for $V_2 = 2$, 1.9, 1.8 and 1.7.

The Ca^{2+} reaches to baseline concentration near the distal end of cells, opposite to the location of its source [75],

$$\lim_{x\to 5}[Ca^{2+}] = [Ca^{2+}]_{\infty} = 0.1\ \mu M. \tag{26}$$

The boundary circumstances for IP_3 molecules are depicted in the following manner [76],

$$\lim_{x\to 5}[IP_3] = 0.16\ \mu M, \tag{27}$$

$$\lim_{x\to 0}[IP_3] = 3\ \mu M,\ t > 0. \tag{28}$$

The boundary conditions pertaining to dopamine regulation were determined by Walters *et al* [77] as phrased in the following manner,

$$\lim_{x\to 0}\left(\frac{\partial[DA]}{\partial x}\right) = 0. \tag{29}$$

$$\lim_{x\to 5}[DA] = 0\ \mu M,\ t > 0. \tag{30}$$

Equations (1)–(30) present the initial boundary value problem (IBVP) formulation for fractional-order PDEs, governing the interacting systems of Ca^{2+}, IP_3 and dopamine. The numerical methodology and analysis of stability have been elucidated in the appendix.

Results and discussion

The graphical representation of the numerical results pertaining to the feedback loop mechanisms of Ca^{2+}, IP_3, and dopamine systems with fractional-order dynamics across spatiotemporal dimensions has been presented. This graphical depiction aids in comprehending various essential cellular processes such as superdiffusion and memory displaying Brownian motion within neuronal cells. Table 1 displays a list of several parameters alongside their corresponding numerical values.

Figure 1 illustrates the spatiotemporal distribution of calcium ion concentration at U_1, U_2, and $U_3 = 1.0$ and V_2 and $V_3 = 2.0$. Additionally, the order of calcium space derivatives (V_1) is observed to vary at 2, 1.9, 1.8, and 1.7. Also, this distribution is influenced by the activity of the buffer and several channels, namely the NCX, PMCA, VGCC, Orai channels, and IP_3R and ryanodine receptors in neuronal cells. The process of calcium ion diffusion, the expulsion of Ca^{2+} ions from the cytosol through the SERCA pump, and the fixing of Ca^{2+} by EGTA buffering mechanisms contribute to a decrease in Ca^{2+} levels along the spatial dimension. Conversely, the influx of calcium from sources and the increase in Orai channel activity leads to a notable rise in Ca^{2+} along the temporal dimension over time. The disparity in $[Ca^{2+}]$ diminishes as the fractional space derivatives V_1 are reduced

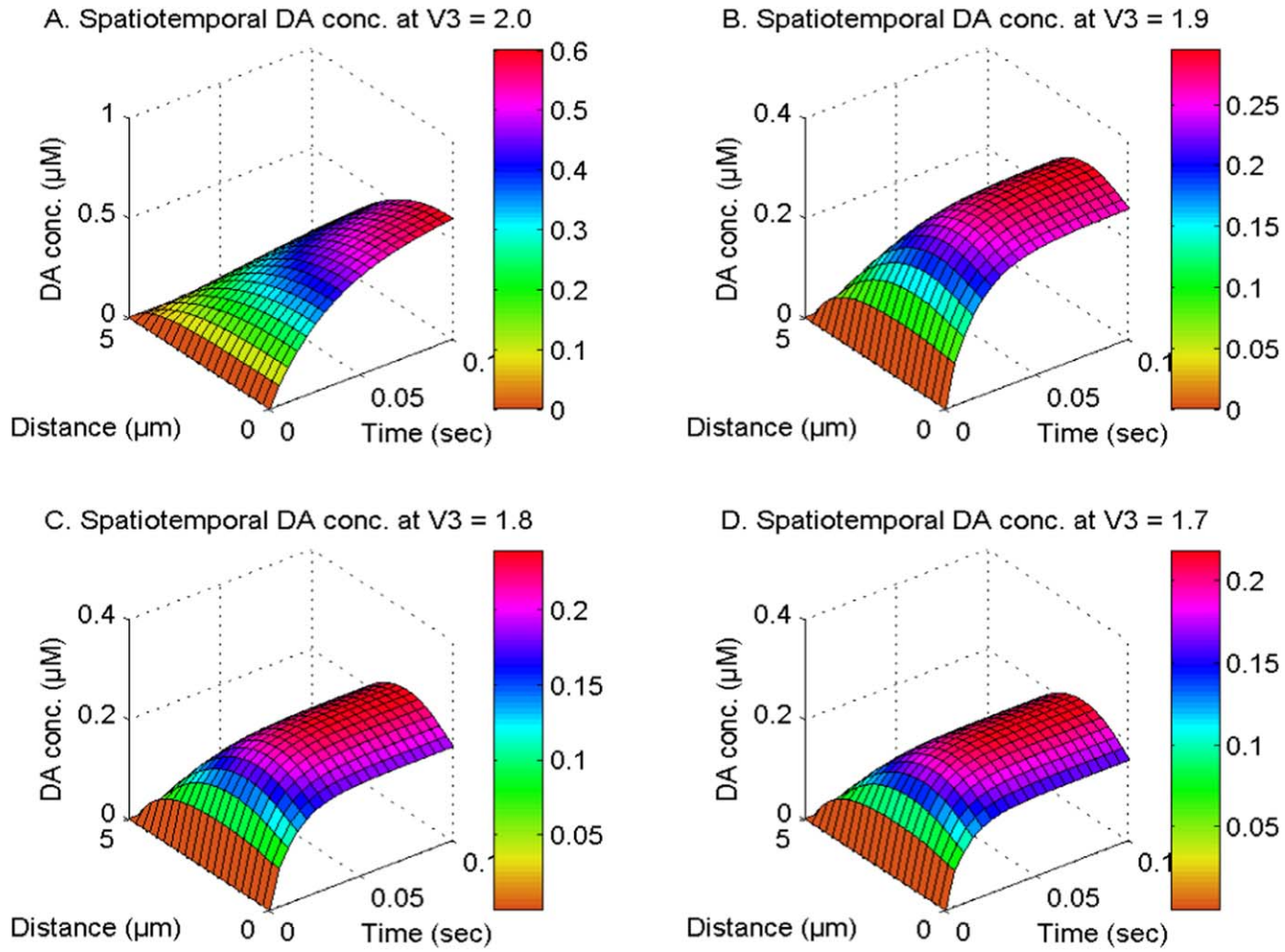

Figure 3. The spatiotemporal DA distribution at U_1, U_2 and $U_3 = 1.0$ and V_1 and $V_2 = 2.0$ with NCX, PMCA, VGCC and Orai channel for $V_3 = 2$, 1.9, 1.8 and 1.7.

from 2 to 1.7 in neurons. The observed range of calcium space derivatives (V_1) transitioning from integer-order (2.0) to fractional-order (1.9, 1.8, and 1.7) is linked to the occurrence of superdiffusion events. This phenomenon amplifies the diffusion process and leads to a drop in the spatiotemporal Ca^{2+} levels. Hence, the phenomenon of superdiffusion exhibited by calcium ions may have a significant impact on mitigating neurotoxicity in disease-related circumstances and maintaining optimal concentration levels.

Figure 2 illustrates the spatiotemporal distribution of IP_3 at U_1, U_2 and $U_3 = 1.0$ and V_1 and $V_3 = 2.0$. The distribution is observed in the existence of NCX, PMCA, VGCC, and Orai channel, while the order of the IP_3 space derivative is considered to be 2, 1.9, 1.8, and 1.7 in neuronal cells. The transportation of inositol trisphosphate molecules and their subsequent breakdown through the actions of kinase and phosphatase enzymes lead to a decrease in the spatial concentration of IP_3 in neuronal cells. The proximity of IP_3 molecule storage to the IP_3-receptor site, which facilitates Ca^{2+} discharge from the ER to the cytosol, is responsible for the temporal increase in IP_3 levels observed in neuronal cells as exhibited in figure 2. The spatiotemporal levels of IP_3

Table 1. Numeric data [42, 74].

Parameter	Value	Parameter	Value
V_{IPR}	8.5 s^{-1}	k^+K_{IP3}	1.5 $\mu M^{-1}\ s^{-1}$
V_{serca}	0.65 $\mu M\ s^{-1}$	λ	0.15 μM
V_{Leak}	0.01 s^{-1}	K_{serca}	30
D_{Ca}	16 $\mu m^2\ s^{-1}$	D_i	0.4 μM
$V_{Production}$	0.075 $\mu M\ s^{-1}$	K_{Ac}	283 $\mu m^2\ s^{-1}$
K_{inh}	1.8 μM	F_E	0.8 μM
V_a	0.001 $\mu M\ s^{-1}$	$K_{Production}$	0.17
V_{ph}	0.02 $\mu M\ s^{-1}$	V_b	0.4 μM
F_C	0.83	f	0.005 $\mu M\ s^{-1}$
V_m	−0.05 V	V_{RyR}	100 Hz
Z_{Ca}	2	P_{Ca}	0.5 $\mu M\ s^{-1}$
T	300 K	R	$4.3 \times 10^{-8}\ m\ s^{-1}$
$[Ca^{2+}]_0$	523.6 μm^3	F	8.31 J/(molK)
Na_i	145 mM	$V_{cytosol}$	96486 C mol^{-1}
V_{max}	6 $\mu M\ s^{-1}$	Na_0	523.6 μm^3
P_{rel}	0.14	K_{rel}	145 mM
n_{RRP}	10	DA_P	700 μM
K_m	0.03 μM		
		0.2 μM	

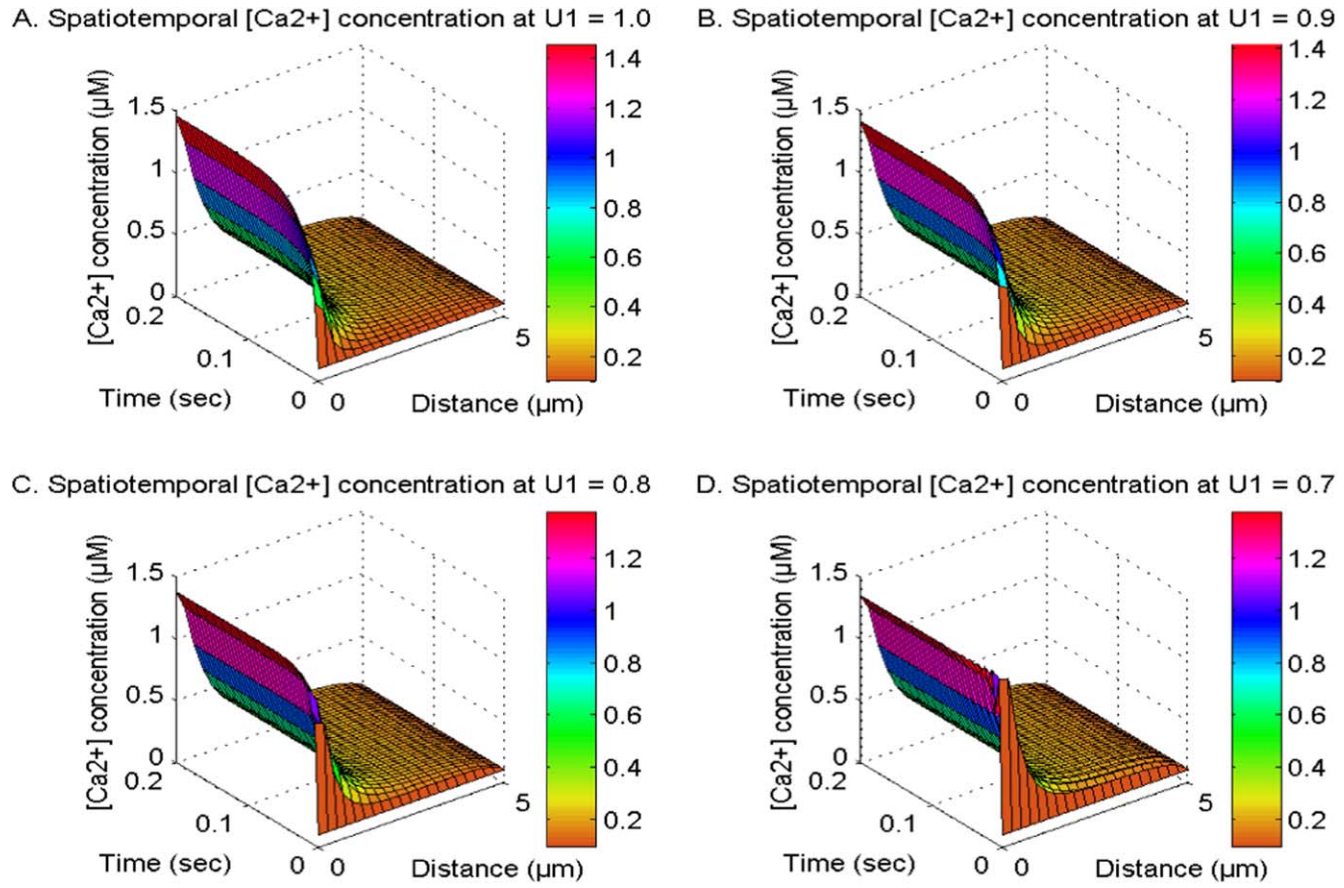

Figure 4. The spatiotemporal Ca^{2+} distribution at V_1, V_2 and $V_3 = 2.0$ and U_2 and $U_3 = 1.0$ with NCX, PMCA, VGCC and Orai channel for $U_1 = 1$, 0.9, 0.8 and 0.7.

molecules exhibit a reduction when the order of space derivative in the IP_3 system transitions from an integer-order ($V_2 = 2.0$) to fractional-order ($V_2 = 1.9$, 1.8, and 1.7). Also, the gaps in [IP_3] diminish when the order of the spatial derivative decreases from $V_2 = 2$ to 1.7. This reduction can be attributed to the occurrence of superdiffusion events in the IP_3 molecules in neuronal cells. The oscillatory behavior of [IP_3] is seen due to a discrepancy in the dynamic regulatory mechanisms of IP_3 in nerve cells during the early time stages. Hence, the superdiffusion process exhibited by IP_3 molecules plays a crucial role in reducing elevated levels of IP_3, as well as its related dynamic ions and molecules such as calcium and dopamine in neurons.

Figure 3 illustrates the spatiotemporal distribution of dopamine at U_1, U_2 and $U_3 = 1.0$ and V_1 and $V_2 = 2.0$. The DA distribution is analyzed in the existence of the NCX, PMCA, VGCC, and Orai channels and the order of the space derivative of the DA system (V_3) is varied at 2.0, 1.9, 1.8, and 1.7 in cells. The spatial levels of dopamine are reduced due to the transportation and degradation of DA molecules, whereas the temporal levels of DA in neuronal cells are increased as a result of DA accumulation. It is noted that the levels of dopamine in neurons are regulated by the superdiffusion processes of individual DA molecules. When the order of the DA space derivative lowers from $V_3 = 2.0$ to 1.8, there is a decrease in the concentration of spatiotemporal DA due to the superdiffusion process in neurons. The spatial [DA] exhibits distinct behavior in the integer-order system compared to the fractional-order system. The maximum spatial [DA] is found near the source location for integer-order spatial derivatives. The spatial DA reaches a maximum concentration at the center of neurons for fractional-order space derivatives, attributable to the excessive diffusion of DA closer to the source within neuronal cells. Therefore, the phenomenon of superdiffusion shown by dopamine molecules may play a notable role in reducing the abnormally high levels of DA and DA-dependent ions and molecules in cells under hazardous conditions.

Figure 4 shows the spatiotemporal calcium ion concentration at V_1, V_2 and $V_3 = 2.0$ and U_2 and $U_3 = 1.0$. This Ca^{2+} distribution is influenced by the active states of NCX, PMCA, VGCC, and Orai channels. The order of time derivative in the Ca^{2+} system (U_1) is evaluated at 1, 0.9, 0.8, and 0.7 in cells. The phenomenon of cell memory exhibiting BM of Ca^{2+} ions is linked to the temporal order of derivative ($0 \leqslant U_1 \leqslant 1$) inside cellular systems. When the temporal derivative order transitions from integer ($U_1 = 1.0$) to fractional (0.9, 0.8, and 0.7), the influence of cell memory exhibiting BM of ions on the Ca^{2+} distribution intensifies in cells. When the value of U_1 declines from 1.0 to 0.7, there is a rise in the spatiotemporal Ca^{2+} levels during the initial period. This elevation is attributed to the cellular memory, which

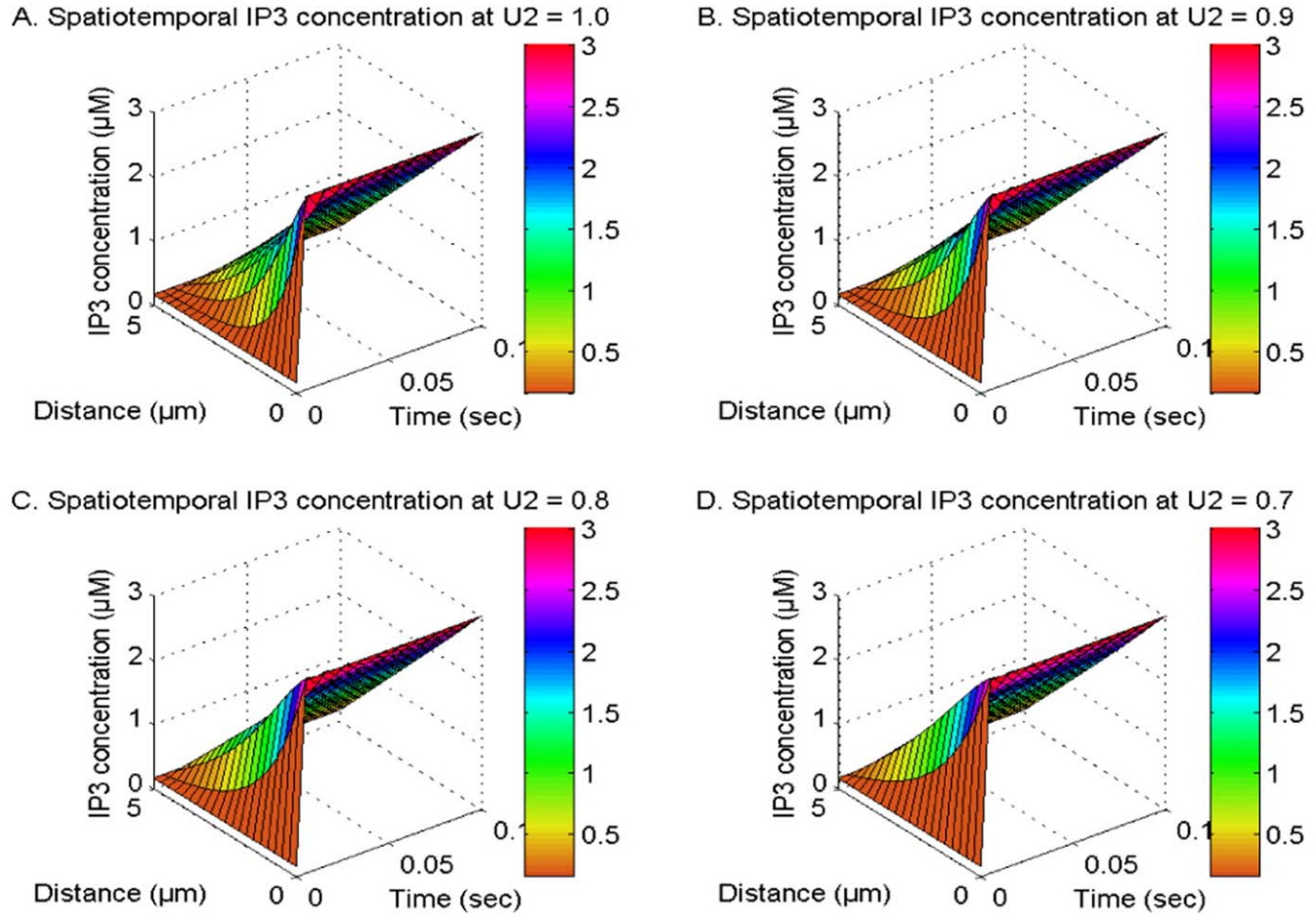

Figure 5. The spatiotemporal IP_3 distribution at V_1, V_2 and $V_3 = 2.0$ and U_1 and $U_3 = 1.0$ with NCX, PMCA, VGCC and Orai channel for $U_2 = 1$, 0.9, 0.8 and 0.7.

induces Brownian motion effects. Also, the significant consequence of cellular memory exhibiting Brownian motion induces disturbances in calcium signaling, which is characterized by oscillatory patterns in Ca^{2+} concentration profiles at $U_1 = 0.7$ as illustrated in figure 4(D). As time advances, the temporal calcium levels reach a state of equilibrium concentration for various time derivatives' orders. This occurs because the cellular control mechanism effectively neutralizes the disruptions induced by memory in neuronal cells. Hence, cellular memory may exert adverse impacts on the calcium signaling pathways and their corresponding dynamics such as IP_3 and DA within neuronal cells.

Figure 5 illustrates the spatiotemporal distribution of IP_3 at V_1, V_2 and $V_3 = 2.0$ and U_1 and $U_3 = 1.0$, considering the existence of PMCA, NCX, VGCC, and Orai channels. The distribution of IP_3 is analyzed for varying orders of time derivative in the IP_3 system, specifically at U_2 values of 1, 0.9, 0.8, and 0.7 in neuronal cells. The fractional order of time derivative in the IP_3 system is associated with the memory and BM of IP_3 molecules. When the time derivative's order (U_2) decreases from an integer value to a fractional value, the elevation in the IP_3 concentration is observed during the initial time noted as a result of memory and BM effects, whereas concentration-decreasing processes attempt to lower $[IP_3]$ levels in neurons. The discrepancies among these mechanisms induce abnormalities in the distribution of IP_3 in the form of fluctuations in neurons. With time, the maintenance of fluctuations in IP_3 distribution at appropriate levels in neuronal cells is achieved through an IP_3 regulatory mechanism. Thus, the presence of cellular memory of IP_3 molecules may contribute to the dysregulation observed in both IP_3 and IP_3-associated signaling systems like Ca^{2+} and dopamine.

Figure 6 illustrates the spatiotemporal distribution of dopamine (DA) at V_1, V_2 and $V_3 = 2.0$ and U_1 and $U_3 = 1.0$, and the order of DA time derivative (U_3) is varied between 1, 0.9, 0.8, and 0.7 in neuronal cells. Also, this distribution is influenced by the presence of NCX, PMCA, VGCC, and Orai channels. When the time derivative of DA reduces from $U_3 = 1.0$ to 0.7, it results in a corresponding decrease in the spatiotemporal DA levels. The influences of the DA cellular memory on the DA distribution differ from the influences of memory of Ca^{2+} and IP_3 on the Ca^{2+} and IP_3 distribution. This is because the DA regulatory mechanism significantly manages the disturbances caused by the cell memory of DA molecules in the initial time. Also, the DA level is dependent on other signaling systems such as calcium and IP_3, whose cell memory is not considered. Thus, the decrease in

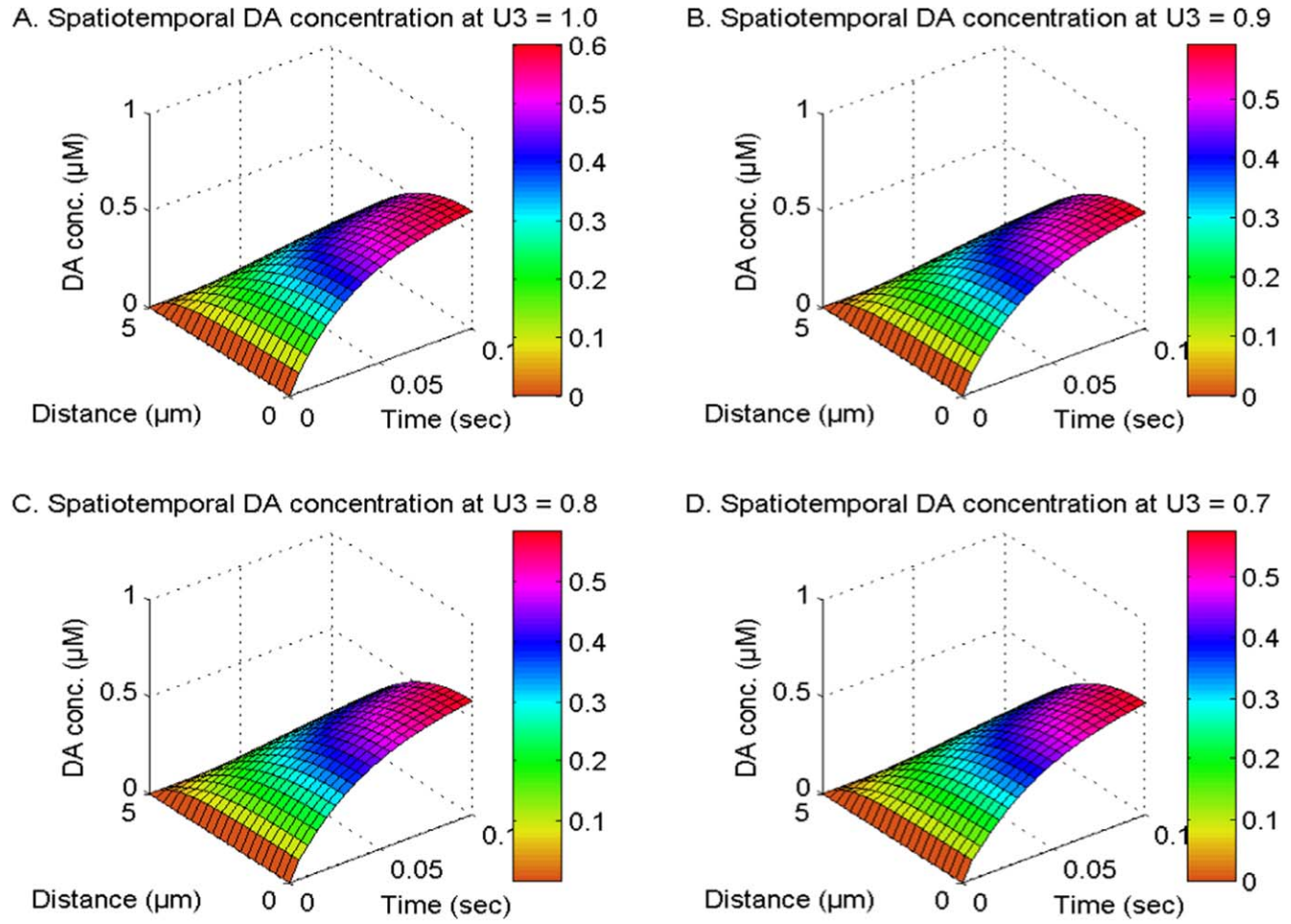

Figure 6. The spatiotemporal DA distribution at V_1, V_2 and $V_3 = 2.0$ and U_1 and $U_2 = 1.0$ with NCX, PMCA, VGCC and Orai channel for $U_3 = 1$, 0.9, 0.8 and 0.7.

spatiotemporal dopamine (DA) levels resulting from cell memory phenomena has been seen in neuronal cells.

Figure 7 depicts the effects of the D_1-receptor on the calcium concentration profiles at different integer-order and fractional-order in neuron cells. The activation of the D_1-receptor stimulates the synthesis of IP_3 molecules, which in turn amplifies the calcium concentration by activating IP_3R in neurons. Deactivating the D_1-receptor decreases the production of IP_3, causing a subsequent decrease in Ca^{2+} levels in cells. The difference in the Ca^{2+} levels for distinct D_1-receptor states exhibits different behavior at integer and fractional order systems within neurons. The functioning of the D_1-receptor is contingent upon the calcium and DA levels within neurons. The modulation of D_1-receptor is directly correlated with dopamine levels and inversely correlated with calcium levels in neurons, which further causes uneven distribution of calcium concerning distinct D_1-receptor states within neurons. The functioning of the D_1-receptor enhances at the fractional-order temporal and spatial derivatives due to memory and superdiffusion processes. Hence, the D_1-receptor significantly influences the allocation of Ca^{2+} across various integer and fractional-order derivatives. Additionally, it exhibits a feedback mechanism that involves Ca^{2+}, IP_3, and DA in neurons.

Figure 8 illustrates the impact of the active and inactive D_1-receptors phases on the spatiotemporal neuronal IP_3 levels. The presence of the D_1-receptor increases the creation of IP_3 molecules, while the absence of the D_1-receptor decreases the generation of IP_3 in neurons. The spatial gradient in IP_3 levels between the active and inactive phases of the D_1-receptor rises from $x = 0\ \mu$m towards the center of cells and subsequently decreases towards the other end ($x = 5\ \mu$m) since the appropriate IP_3 concentration levels are maintained at both the boundaries within neurons. The temporal disparities in IP_3 concentrations between active and inactive D_1-receptor phases increase throughout time and reach a state of balance at various locations within neurons. The difference in IP_3 concentration levels increases when the fractional time derivatives (U_1, U_2 and $U_3 = 0.9$) are considered due to the memory effects of ions and molecules within neurons. Furthermore, the molecules exhibit superdiffusion, which leads to a reduction in the differences in IP3 concentration levels. This effect is observed when the fraction space derivatives (V_1, V_2 and $V_3 = 1.9$) are taken into account.

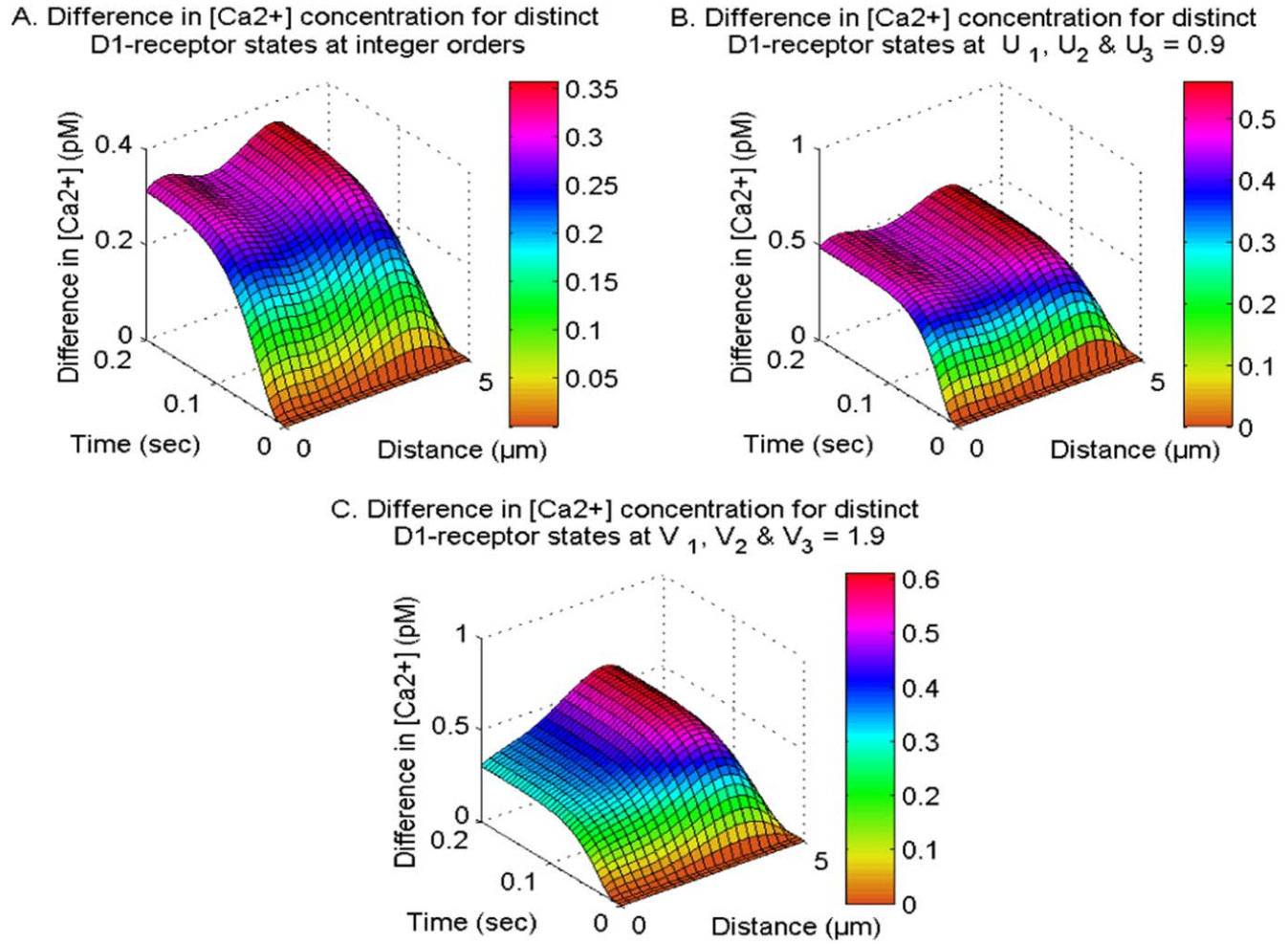

Figure 7. The difference in spatiotemporal Ca^{2+} distribution at integer and fractional orders with NCX, PMCA, VGCC and Orai channel for distinct D1-receptor states.

Therefore, the D_1-receptor has a substantial impact on the distribution of IP_3 at different integer as well as fractional-order derivatives, and it also demonstrates a feedback loop involving Ca^{2+}, IP_3, and DA in neurons.

Figure 9 displays the spatiotemporal Ca^{2+} concentration for distinct buffers namely EGTA and Calbindin-D_{28K} in neurons. The buffer molecule exhibits an affinity to the excess cytosolic Ca^{2+} ions to bind them, hence reducing the cytosolic Ca^{2+} within cells. Upon analysis of the distinct buffers, it is evident that neuronal cells have a higher reduction in calcium levels for the Calbindin-D_{28K} buffer as compared to the EGTA buffer. The Calbindin-D_{28K} buffer has a higher affinity for binding calcium ions in contrast to the EGTA buffer, which results in the temporal [Ca^{2+}] profile reaching steady-state more rapidly than the EGTA buffer within the cell. Similarly in figure 10, the spatiotemporal IP_3 and DA production fluxes, which are reliant on Ca^{2+} levels, also demonstrate a comparable pattern for EGTA and Calbindin-D_{28K} buffers in neurons. In the case of Calbindin-D_{28K} buffer, there is a decreased amount of IP_3 and DA production in cells. Hence, the Calbindin-D_{28K} buffer plays a significant role in maintaining the appropriate levels of calcium, IP_3, and DA in situations involving neurotoxicity and illness.

Table 2. Absolute relative error approximations for [Ca^{2+}], [IP_3] and [DA] distribution.

GSI	Errors for [Ca^{2+}] 0 μm	Errors for [IP_3] 0.25 μm	Errors for [DA] 0 μm
10 and 11	0.053521%	0.88%	12.20%
20 and 21	0.0055890%	0.29%	6.67%
50 and 51	$1.9631 \times 10^{-4\%}$	0.011438%	0.72%
100 and 101	7.5399×10^{-7}%	4.4128×10^{-5}%	0.0079433%

Table 2 displays the absolute relative approximate errors for Ca^{2+}, IP_3, and DA concerning GSI. At GSI = 100, the lowest accuracy and maximum error of the model for Ca^{2+}, IP_3, and DA are 99.9920567% and 0.0079433%, respectively.

The numerical results of the integer-order Ca^{2+} and IP_3 systems are displayed in table 3. These findings are consistent with the documented results [42] at a time of 50 s, indicating a good agreement between the current findings and existing research. The root mean square errors for Ca^{2+} and IP_3 were determined to be 0.0035 and 0.000 119 95, sequentially.

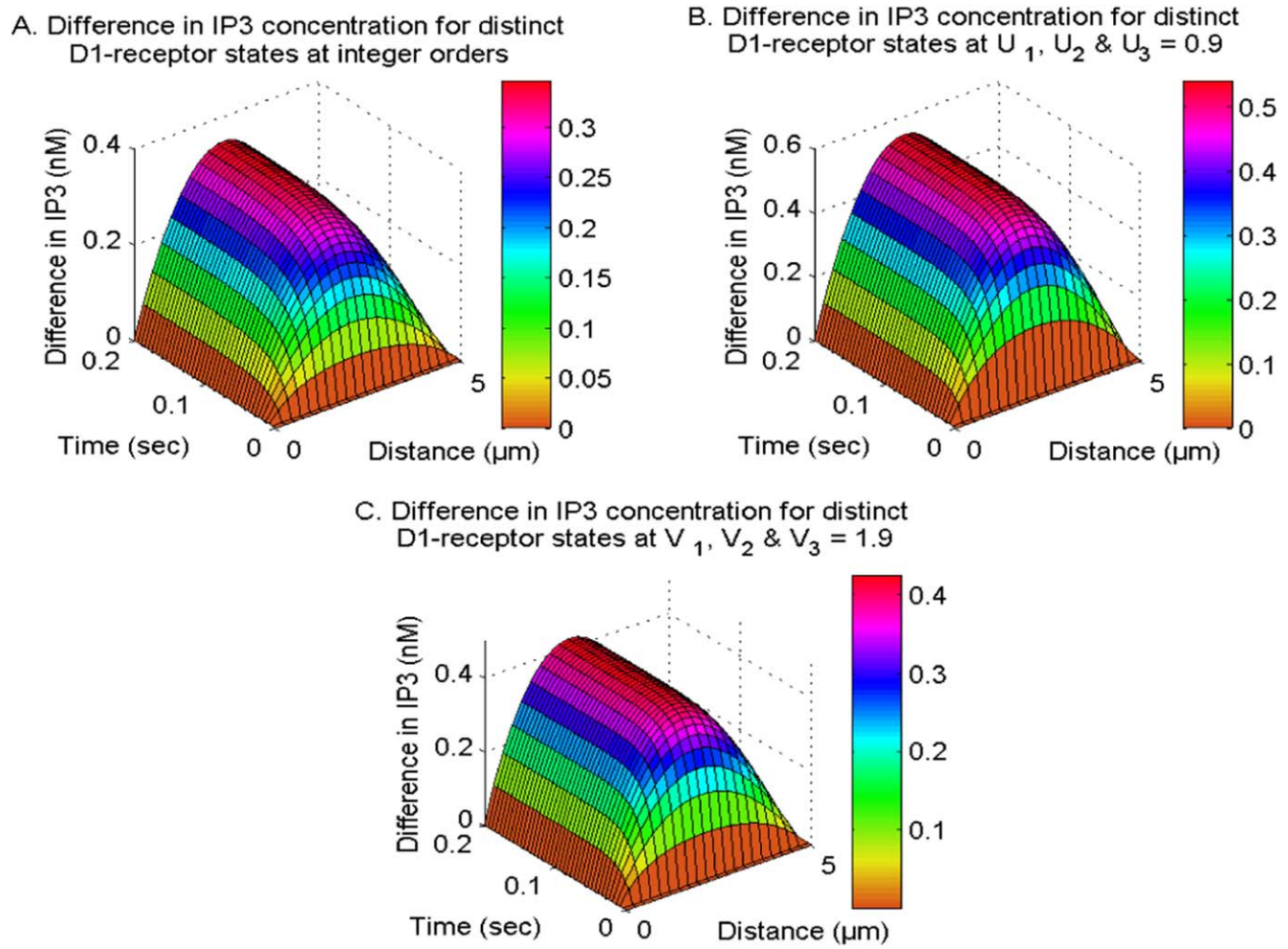

Figure 8. The difference in spatiotemporal IP_3 distribution at integer and fractional orders with NCX, PMCA, VGCC and Orai channel for distinct D1-receptor states.

Table 3. $[Ca^{2+}]$ and $[IP_3]$ at $t = 50$ s compared to Wagner *et al* [42].

Position (μm)	Ca^{2+} levels [42]	Ca^{2+} levels (present results)	IP_3 levels [42]	IP_3 levels (present results)
0	1.350000000000000	1.338361848552280	0.500000000000000	0.500000000000000
0.5	1.232315043169371	1.236870382828057	0.466142830711937	0.466206313913817
1	1.115735280749170	1.119398214539027	0.432270696317190	0.432382728076332
2	0.878398731277883	0.880712373555526	0.364452905490556	0.364617532532743
3	0.628405810701451	0.629765718417450	0.296501658993935	0.296661310337345
5	0.100000000000000	0.100000000000000	0.160000000000000	0.160000000000000

Nevertheless, the lack of experimental documentation on the kinetics of fractional-order calcium and IP_3 is a significant challenge in terms of attaining thorough validation. Also, the numerical outcomes related to the fractional concentration of calcium ions, IP_3, and dopamine signaling mechanisms within neuronal cells exhibit conformity with biophysical realities.

Tables 4 and 5 depict the comparison in the Ca^{2+}, IP_3 and DA levels (in μM) among three interacting systems: Ca^{2+}, IP_3 and DA, with two interacting systems including Ca^{2+} and IP_3 and Ca^{2+} and DA at distinct neuronal sites. The previous fractional-order model of the two signaling systems of Ca^{2+} and IP_3 included the bi-directional feedback between calcium and IP_3 in neurons. However, the influence of the ryanodine receptor on the interacting calcium and IP_3 was not addressed in the prior fractional-order model. The dynamics of fractional-order calcium and dopamine, together with the effects of the ryanodine receptor, were included; however, there is solely unidirectional feedback between calcium and dopamine in neurons. The present study establishes the feedback loop mechanism among fractional-order Ca^{2+}, IP_3, and DA signaling systems by integrating the D_1-receptor in the regulation of IP_3 in neurons. The present work incorporates various essential cellular processes namely the PMCA channel, Orai channel,

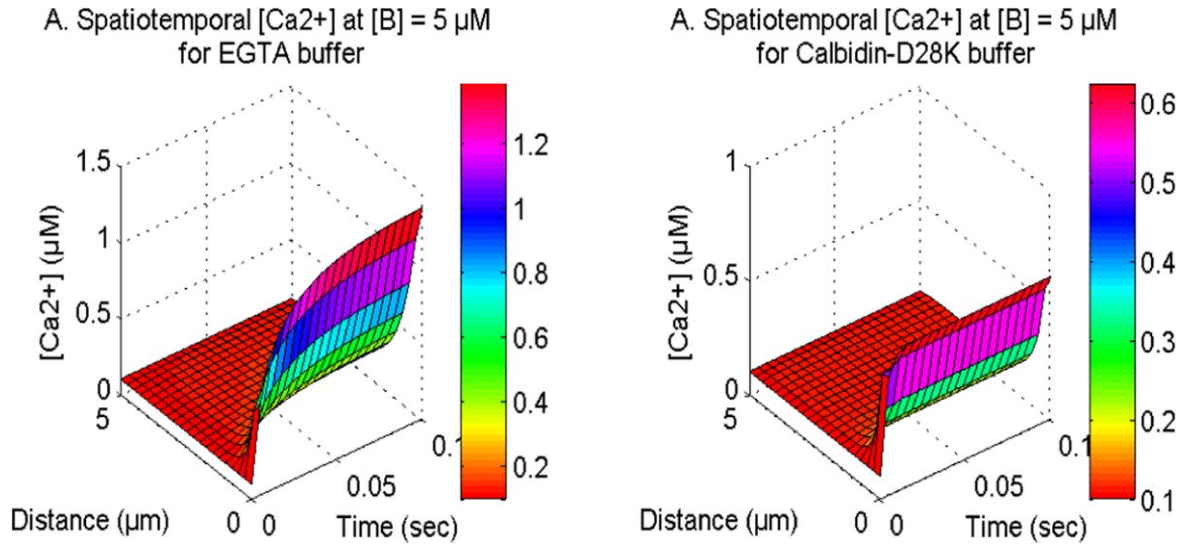

Figure 9. The spatiotemporal Ca^{2+} distribution with NCX, PMCA, VGCC and Orai channel for EGTA and Calbidin-D_{28K} buffers.

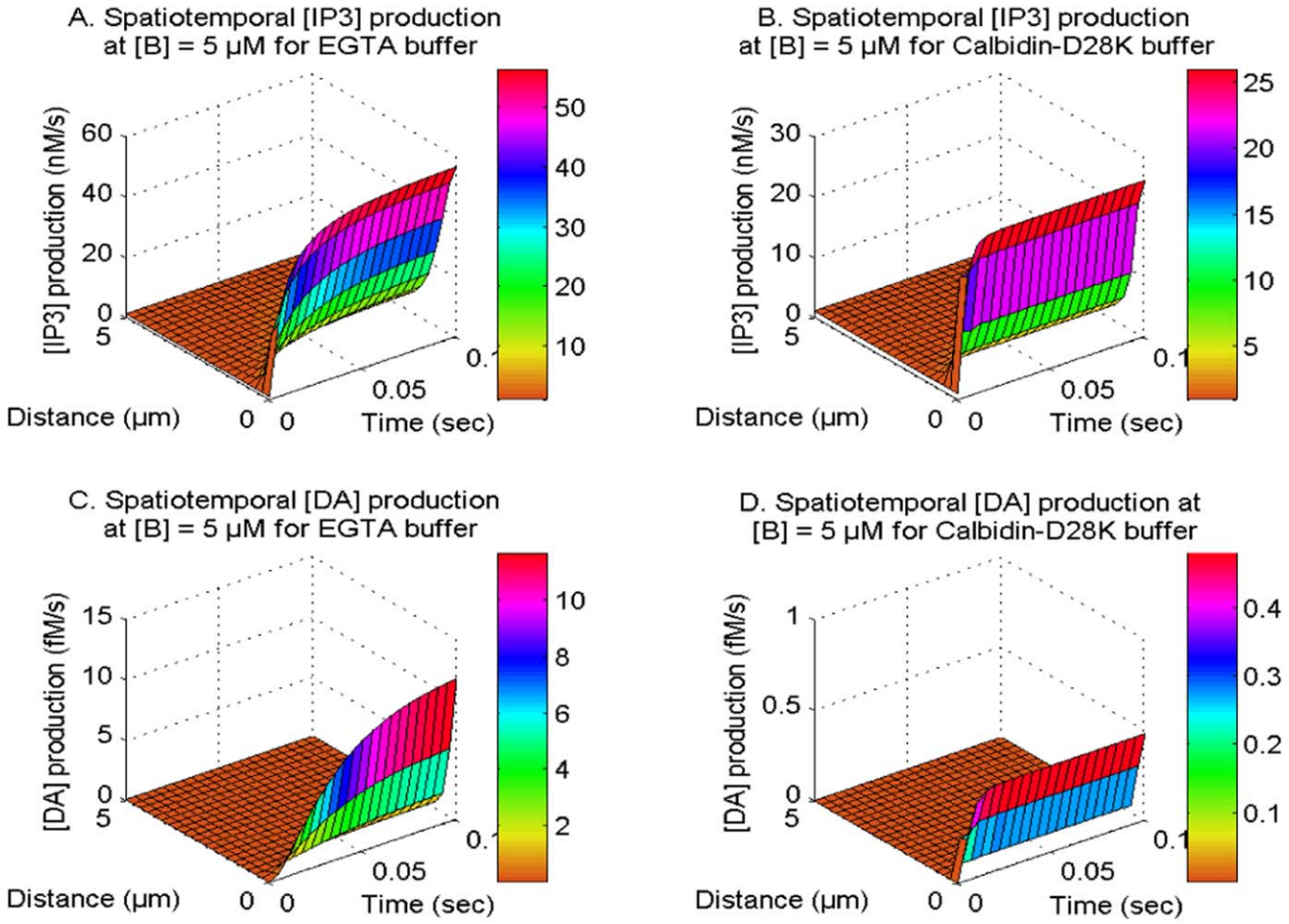

Figure 10. The spatiotemporal IP_3 and DA production with NCX, PMCA, VGCC and Orai channel for EGTA and Calbidin-D_{28K} buffers.

VGCC, and NCX, which control Ca^{2+}, IP_3, and DA at optimal levels in neurons. The impacts of these pathways were not present in the previously reported research. Consequently, the interplay of Ca^{2+}, IP_3, and DA signaling pathways, in conjunction with biological mechanisms such as the D_1-receptor, PMCA channel, Orai channel, RyR, VGCC, and NCX, renders the current study more advanced than previously published research.

Table 4. Comparison of $[Ca^{2+}]$ in three signaling systems of Ca^{2+}, IP_3, and DA with the $[Ca^{2+}]$ in two interacting systems of Ca^{2+} and IP_3 and Ca^{2+} and DA.

Locations (in μm)	$[Ca^{2+}]$ for two signaling systems; Ca^{2+} and IP_3	$[Ca^{2+}]$ for two signaling systems; Ca^{2+} and DA	$[Ca^{2+}]$ for three signaling systems; Ca^{2+}, IP_3, and DA
0	1.59352626311615	1.67374166702743	1.39639145777306
1	0.959594060751098	1.10734892213237	0.444646823496717
2	0.583964456594164	0.775884667935086	0.199507243264428
3	0.360415236709176	0.573624721540783	0.152937005272446
4	0.212589240812298	0.377880288715064	0.136796466146167
5	0.1	0.1	0.1

Table 5. Comparison of $[IP_3]$ and [DA] in three signaling systems of Ca^{2+}, IP_3, and DA with the $[IP_3]$ and [DA] in two interacting systems of Ca^{2+} and IP_3 and Ca^{2+} and DA.

Locations (in μm)	IP_3 for two signaling systems; Ca^{2+} and IP_3	IP_3 for three signaling systems; Ca^{2+}, IP_3, and DA	DA for two signaling systems; Ca^{2+} and DA	DA for three signaling systems; Ca^{2+}, IP_3, and DA
0	3	3	0.633949375794030	0.634047185204713
1	2.43213661177129	2.43164738874235	0.611019641480479	0.611104126486061
2	1.86430790558617	1.86361274208202	0.538408754743416	0.538474355261389
3	1.29639654811965	1.29574921058797	0.412791833315504	0.412836720211876
4	0.728322817076785	0.727927224597782	0.233790129029834	0.233813079757628
5	0.16	0.16	0	0

Conclusion

A mathematical model has been framed for interactive systems of nonlinear calcium, IP_3, and dopamine, utilizing a fractional-order approach along spatial and temporal dimensions. The CN method with the Grunwald technique for fractional spatial derivatives and the L1 scheme for fractional temporal derivatives in combination with GSI were employed to get numerical findings. The L1 scheme is exceptionally resilient and effective for the analysis of fractional-order differential equations. The fundamental characteristic of the L1 scheme is its capacity to integrate a memory trail that records and assimilates all previous occurrences, essential for simulating the dynamics. Earlier researchers examined the fractional-order reaction-diffusion models of calcium and DA incorporating unidirectional feedback in neurons. However, no fractional-order model has been documented about the bidirectional feedback process between calcium and dopamine in neuronal cells. The influence of DA on calcium signaling is facilitated by the integration of IP_3 signaling molecules, as DA signaling plays a crucial role in the synthesis of IP_3 molecules. The interplay of IP_3 signaling with calcium and the dopamine system generates a feedback loop among these three dynamic systems. No study is presently documented on the interacting fractional-order systems of Ca^{2+}, IP_3 and DA in neuronal cells. Also, the current model offers novel viewpoints on the implications of superdiffusion processes and cellular memory, which exhibit BM on the cooperation of fractional-order nonlinear dynamics of Ca^{2+}, IP_3, and DA in neurons. To assess the model's performance, the absolute relative approximation errors for Ca^{2+}, IP_3, and DA concentrations in neurons at various sites have been computed across multiple GSI. At 100 iterations, the model's minimum accuracy and maximum error for Ca^{2+}, IP_3, and DA are recorded at 99.9920567% and 0.0079433%, respectively. The spectral radius has been calculated to assess stability and is found to be less than 1, indicating the unconditional stability of the numerical techniques applied.

From the aforementioned results, the following basic conclusions can be drawn:

1. The superdiffusion phenomenon is a concentration-reducing mechanism. Enhanced diffusion promotes a more comprehensive and efficient reduction of intracellular Ca^{2+} levels through improved accessibility to binding sites and buffers, effective removal by intracellular organelles, membrane extrusion mechanisms, and feedback regulation.
2. Cellular memory induces an increase in the concentration of ions and molecules during the early period. Over time, it begins to diminish the concentration levels of ions and molecules within neurons.
3. Various buffer types, specifically EGTA and Calbindin-D28K, diminish cytosolic calcium ion concentrations in differing amounts due to their distinct interaction rates with calcium in neurons.

The obtained numerical results have led to the following novel conclusions:

1. A significant decrease in the spatiotemporal concentration levels of Ca^{2+}, IP_3, and dopamine has been observed due to the superdiffusion mechanism in neuronal cells. In conditions associated with disease and characterized by high concentrations, the cell may use superdiffusion phenomena as an approach for reducing neurotoxicity.

Any disturbances in the superdiffusion process can result in increased levels of Ca^{2+}, IP_3, and dopamine, leading to the disruption of the interactive spatiotemporal dynamical system involving these ions and molecules.

2. The impact of DA cell memory on DA concentration levels varies from the impact of calcium and IP_3 memory on calcium and IP_3 concentration in neurons. The reason for this behavior can be attributed to the regulatory mechanism of dopamine, which effectively controls the disruptions induced by cell memory and Brownian motion of DA molecules within neuronal cells during initial time.
3. The D_1-receptor influences the concentration of calcium, IP_3, and DA in neurons. The functioning of D_1-receptor at fractional-order space and time derivatives significantly differs from the integer-order space and time derivatives within neurons due to the memory and accelerated diffusion phenomena and the same is visible in our findings.
4. The neuronal cells experience a greater decrease in calcium levels concerning Calbindin-D_{28K} buffer compared to the EGTA buffer, which further leads to reduced IP_3 and DA synthesis in neuronal cells.

Therefore, it may be inferred that the phenomenon of superdiffusion and memory which involves the BM of calcium, IP_3, and DA have crucial functions in governing the dynamical signaling systems of neuronal Ca^{2+}, IP_3 and dopamine. The deregulation of any or all of these pathways can result in neurotoxic circumstances and contribute to the progression of disease-associated conditions such as AD.

The interaction of three signaling ions and molecules namely calcium, IP_3, and DA has been considered in the proposed model. However, the current study establishes a foundation for future investigations into the dynamic interactions of critical neuronal signaling molecules, including Aβ, PLC, and ATP, with nonlinear calcium, IP_3, and DA dynamics in both healthy and pathological neuronal states. Moreover, the intricate connections of additional essential signaling molecules with the calcium, IP_3, and DA systems will provide a more precise comprehension of several illnesses, including Alzheimer's disease and Parkinson's disease.

The CN approach, Grunwald and L1 schemes, and GS iterations have demonstrated significant efficacy in obtaining essential insights into the interactive Ca^{2+}, IP_3, and DA signaling systems within neuronal cells. This study provides insights into the roles of superdiffusion and cellular memory signaling molecules, as well as the essential signaling mechanisms regulating the concentration levels of calcium, IP_3, and DA in neurons. Also, the information acquired through these models on the basic mechanisms and events linked with disease-related states can be valuable to biomedical researchers in the advancement of diagnostic and therapeutic interventions.

Competing interests

Both authors of this paper assert that they have no conflicting interests.

Appendix. Model equations summary

The fractional derivatives along space in equations (1), (14) and (20) exhibit the utilization of the CN method in conjunction with the Grunwald formula as follows [78],

$$\frac{\partial^{V_1}[Ca^{2+}]}{\partial x^{V_1}} = \left(\sum_{k=0}^{i+1}\left(\frac{1}{2h^{V_1}}g1_k[Ca^{2+}]_{i-k+1}^{j} + \frac{1}{2h^{V_1}}g1_k[Ca^{2+}]_{i-k+1}^{j+1}\right), \quad (31)$$

$$\frac{\partial^{V_2}[IP_3]}{\partial x^{V_2}} = \sum_{k=0}^{i+1}\left(\frac{1}{2h^{V_2}}g2_k[IP_3]_{i-k+1}^{j} + \frac{1}{2h^{V_2}}g2_k[IP_3]_{i-k+1}^{j+1}\right), \quad (32)$$

$$\frac{\partial^{V_3}[DA]}{\partial x^{V_3}} = \sum_{k=0}^{i+1}\left(\frac{1}{2h^{V_3}}g3_k[DA]_{i-k+1}^{j} + \frac{1}{2h^{V_3}}g3_k[DA]_{i-k+1}^{j+1}\right), \quad (33)$$

Where, the h denotes the spatial increment for $i = 1, 2, 3,\ldots, K-1$. The normalized Grunwald weights referred to as $g1_k$, $g2_k$, and $g3_k$, are contingent upon the index k and the orders V_1, V_2, and V_3, in a sequential manner. The representation of these weights is as follows:

$$g1_k = \frac{\Gamma(k - V_1)}{\Gamma(-V_1)\Gamma(k+1)}, \quad (34)$$

$$g2_k = \frac{\Gamma(k - V_2)}{\Gamma(-V_2)\Gamma(k+1)}, \quad (35)$$

$$g3_k = \frac{\Gamma(k - V_3)}{\Gamma(-V_3)\Gamma(k+1)}, \quad (36)$$

The fractional derivatives along time in equations (1), (14) and (20) exhibit the utilization of the L1 scheme as follows [79],

$$\frac{\partial^{U_1}[Ca^{2+}]}{\partial t^{U_1}} = \frac{1}{\Gamma(2-U_1)}\sum_{k=0}^{j}\frac{b1_k([Ca^{2+}]_i^{j+1-k} - [Ca^{2+}]_i^{j-k})}{(\Delta t)^{U_1}} \quad (37)$$

$$\frac{\partial^{U_2}[IP_3]}{\partial t^{U_2}} = \frac{1}{\Gamma(2-U_2)}\sum_{k=0}^{j}\frac{b2_k([IP_3]_i^{j+1-k} - [IP_3]_i^{j-k})}{(\Delta t)^{U_2}}, \quad (38)$$

$$\frac{\partial^{U_3}[DA]}{\partial t^{U_3}} = \frac{1}{\Gamma(2-U_3)}\sum_{k=0}^{j}\frac{b3_k([DA]_i^{j+1-k} - [DA]_i^{j-k})}{(\Delta t)^{U_3}}, \quad (39)$$

where

$$b1_k = (k+1)^{1-U_1} - (k)^{1-U_1}, \quad (40)$$

$$b2_k = (k+1)^{1-U_2} - (k)^{1-U_2}, \quad (41)$$

$$b3_k = (k+1)^{1-U_3} - (k)^{1-U_3}. \quad (42)$$

Considering $C = [Ca^{2+}]$, $P = [IP_3]$ and $\beta = [DA]$ and employing equations (31) and (37) within equation (1), we obtain

$$\frac{1}{\Gamma(2-U_1)}\sum_{k=0}^{j}\frac{b1_k(C_i^{j+1-k}-C_i^{j-k})}{(\Delta t)^{U_1}} = D_{\mathrm{Ca}}\frac{1}{2h^{V_1}}\sum_{k=0}^{i+1}\frac{\Gamma(k-V_1)}{\Gamma(-V_1)\Gamma(k+1)}C_{i-k+1}^{j} + \frac{1}{2h^{V_1}}\sum_{k=0}^{i+1}\frac{\Gamma(k-V_1)}{\Gamma(-V_1)\Gamma(k+1)}C_{i-k+1}^{j+1}$$
$$+\frac{1}{F_C}\left(\begin{array}{l} V_{\mathrm{IPR}}m^3h^3(C_{\mathrm{ER}}-C_i^j) - V_{\mathrm{SERCA}}\left(\dfrac{(C_i^j)^2}{(C_i^j)^2+(K_{\mathrm{SERCA}})^2}\right) \\ +V_{\mathrm{LEAK}}(C_{\mathrm{ER}}-C_i^j) + V_{RyR}P_0(C_{\mathrm{ER}}-C_i^j) + K_\beta(\beta_i^j)^m \end{array}\right)$$
$$-K^+[B]_\infty(C_i^j-C_\infty) - V_{\mathrm{PMCA}}\left(\frac{(C_i^j)^2}{(C_i^j)^2+(K_{\mathrm{PMCA}})^2}\right). \tag{43}$$

Employing equations (32) and (38) within equation (14), we obtain

$$\frac{1}{\Gamma(2-U_2)}\sum_{k=0}^{j}\frac{b2_k(P_i^{j+1-k}-P_i^{j-k})}{(\Delta t)^{U_2}} = D_i\frac{1}{2h^{V_2}}\sum_{k=0}^{i+1}\frac{\Gamma(k-V_2)}{\Gamma(-V_2)\Gamma(k+1)}P_{i-k+1}^{j} + \frac{1}{2h^{V_2}}\sum_{k=0}^{i+1}\frac{\Gamma(k-V_2)}{\Gamma(-V_2)\Gamma(k+1)}P_{i-k+1}^{j+1}$$
$$+\frac{1}{F_c}\left(\begin{array}{l} V_{\mathrm{production}}\left(\dfrac{(C_i^j)^2}{(C_i^j)^2+(K_{\mathrm{production}})^2}\right) - \lambda V_a\left(1-\left(\dfrac{C_i^j}{C_i^j+0.39}\right)\right)\left(\dfrac{P_i^j}{P_i^j+2.5}\right) \\ -\lambda V_b\left(\dfrac{C_i^j}{C_i^j+0.39}\right)\left(\dfrac{P_i^j}{P_i^j+0.5}\right) - \lambda V_{\mathrm{ph}}\left(\dfrac{P_i^j}{P_i^j+30}\right) \end{array}\right)$$
$$+V_{\mathrm{DA}}\frac{(\beta_i^j)^\gamma}{(\beta_i^j)^\gamma+\left(K_{\mathrm{DA}}+K_P\frac{C_i^j}{C_i^j+K_{P1}}\right)^\gamma}. \tag{44}$$

Employing equations (33) and (39) within equation (20), we obtain

$$\frac{1}{\Gamma(2-U_3)}\sum_{k=0}^{j}\frac{b3_k(\beta_i^{j+1-k}-\beta_i^{j-k})}{(\Delta t)^{U_3}} = D_{\mathrm{DA}}\frac{1}{2h^{V_3}}\sum_{k=0}^{i+1}\frac{\Gamma(k-V_3)}{\Gamma(-V_3)\Gamma(k+1)}\beta_{i-k+1}^{j} + \frac{1}{2h^{V_3}}\sum_{k=0}^{i+1}\frac{\Gamma(k-V_3)}{\Gamma(-V_3)\Gamma(k+1)}\beta_{i-k+1}^{j+1}$$
$$+\psi.n_{\mathrm{RRP}}.P_{\mathrm{rel}}\left(\frac{(C_i^j)^4}{(C_i^j)^4+K_{\mathrm{rel}}^4}\right)+[\mathrm{DA}]_P f - \frac{V_{\max}\beta_i^j}{(\beta_i^j+K_m)}. \tag{45}$$

From equation (26), we obtain,

$$\frac{1}{\Gamma(2-U_1)}\sum_{k=0}^{j}\frac{b1_k(C_i^{j+1-k}-C_i^{j-k})}{(\Delta t)^{U_1}} = D_{\mathrm{Ca}}\left(\frac{1}{2h^{V_1}}\sum_{k=0}^{i+1}g1_kC_{i-k+1}^{j} + \frac{1}{2h^{V_1}}\sum_{k=0}^{i+1}g1_kC_{i-k+1}^{j+1}\right) + d1(C_i^j,P_i^j,\beta_i^j) + f_i^{j+1}, \tag{46}$$

$$\sum_{k=0}^{j}b1_k(C_i^{j+1-k}-C_i^{j-k}) = D_{\mathrm{Ca}}\frac{\Gamma(2-U_1)(\Delta t)^{U_1}}{2h^{V_1}}\left(\sum_{k=0}^{i+1}g1_kC_{i-k+1}^{j} + \sum_{k=0}^{i+1}g1_kC_{i-k+1}^{j+1}\right)$$
$$+\Gamma(2-U_1)(\Delta t)^{U_1}d1(C_i^j,P_i^j,\beta_i^j) + \Gamma(2-U_1)(\Delta t)^{U_1}f1_i^{j+1}. \tag{47}$$

Defining, $B1 = D_{\mathrm{Ca}}\frac{\Gamma(2-U_1)(\Delta t)^{U_1}}{2h^{V_1}}$, then equation (47) can be expressed in the following manner

$$\sum_{k=0}^{j}b1_k(C_i^{j+1-k}-C_i^{j-k}) = B1\left(\sum_{k=0}^{i+1}g1_kC_{i-k+1}^{j} + \sum_{k=0}^{i+1}g1_kC_{i-k+1}^{j+1}\right) + \Gamma(2-U_1)(\Delta t)^{U_1}d1(C_i^j,P_i^j,\beta_i^j)$$
$$+\Gamma(2-U_1)(\Delta t)^{U_1}f1_i^{j+1}, \tag{48}$$

$$b1_0(C_i^{j+1}-C_i^j) + b1_1(C_i^j-C_i^{j-1}) + \sum_{k=2}^{j}b1_k(C_i^{j+1-k}-C_i^{j-k}) = B1g1_0C_{i+1}^{j} + B1g1_1C_i^j + B1\left(\sum_{k=2}^{i}g1_kC_{i-k}^{j}\right) + B1g1_0C_{i+1}^{j+1}$$
$$+B1g1_1C_i^{j+1} + B1g1_2C_{i-1}^{j+1} + B1\left(\sum_{k=3}^{i}g1_kC_{i-k}^{j+1}\right)$$
$$+\Gamma(2-U_1)(\Delta t)^{U_1}d1(C_i^j,P_i^j,\beta_i^j) + \Gamma(2-U_1)(\Delta t)^{U_1}f1_i^{j+1}, \tag{49}$$

$$-B1g1_0C_{i+1}^{j+1}+(b1_0-B1g1_1)C_i^{j+1}-B1g1_2C_{i-1}^{j+1}-B1\left(\sum_{k=3}^{i+1}g1_kC_{i-k+1}^{j+1}\right)=B1g1_0C_{i+1}^{j}+(B1g1_1+b1_0-b1_1)C_i^{j}$$
$$+b1_1C_i^{j-1}+B1\left(\sum_{k=2}^{i+1}g1_kC_{i-k+1}^{j}\right)-\sum_{k=2}^{j}b1_k(C_i^{j+1-k}-C_i^{j-k})+\Gamma(2-U_1)(\Delta t)^{U_1}d1(C_i^j,P_i^j,\beta_i^j)+\Gamma(2-U_1)(\Delta t)^{U_1}f1_i^{j+1}, \tag{50}$$

Where, the nonlinear terms for equation (43) are represented by $d1(C_i^j, P_i^j, \beta_i^j)$.

The equation (50) shows a nonlinear equations system, which is reformulated as follows:

$$\bar{A}1\,\bar{C}^{j+1}=\bar{M}1\,\bar{C}^{j}+\left(b1_1C_i^{j-1}-\sum_{k=2}^{j}b1_k(C_i^{j+1-k}-C_i^{j-k})\right)$$
$$+\Gamma(2-U_1)(\Delta t)^{U_1}d1(C_i^j,P_i^j,\beta_i^j)+\Gamma(2-U_1)(\Delta t)^{U_1}\bar{F}1^{j+1}, \tag{51}$$

where

$$\bar{C}^{j+1}=[C_0{}^{j+1},\,C_1{}^{j+1},\,C_2{}^{j+1},\,...,C_K{}^{j+1}]^{\mathrm{T}}. \tag{52}$$

$$\bar{C}^{j}=[0,\,C_1{}^{j},\,C_2{}^{j},\,...,C_{K-1}{}^{j}]^{\mathrm{T}}. \tag{53}$$

$$\bar{F}1^{j}=[0,\,f1_1^j,\,f1_2^j,\,...,f1_{K-1}^j]^{\mathrm{T}}. \tag{54}$$

The coefficients matrix is represented by $\bar{A}1=[A1_{i,j}]$ for $i, j=1, 2,\ldots, K-1$ as,

$$A1_{i,j}=\begin{Bmatrix}0 & \text{When } j\geqslant i+2\\ -g1_0B1 & \text{When } j=i+1\\ b1_0-g1_1B1 & \text{When } j=i\\ -g1_2B1 & \text{When } j=i-1\\ -g1_{i-j+1}B1 & \text{When } j\leqslant i-1\end{Bmatrix}. \tag{55}$$

Similarly, by employing the L1 formula for time dimension and the CN method with Grunwald approach for spatial dimension in equation (44) as follows,

$$\bar{A}2\bar{P}^{j+1}=\bar{M}2\bar{P}^{j}+\left(b2_1P_i^{j-1}-\sum_{k=2}^{j}b2_k(P_i^{j+1-k}-P_i^{j-k})\right)+\Gamma(2-U_2)(\Delta t)^{U_2}d2(C_i^j,P_i^j,\beta_i^j)+\Gamma(2-U_2)(\Delta t)^{U_2}\bar{F}2^{j+1}. \tag{56}$$

The coefficients matrix is expressed by $\bar{A}2=[A2_{i,j}]$ for $i, j=1, 2, 3,\ldots, K-1$ as follows,

$$A2_{i,j}=\begin{Bmatrix}0 & \text{When } j\geqslant i+2\\ -g2_0B2 & \text{When } j=i+1\\ b2_0-g2_1B2 & \text{When } j=i\\ -g2_2B2 & \text{When } j=i-1\\ -g2_{i-j+1}B2 & \text{When } j\leqslant i-1\end{Bmatrix}, \tag{57}$$

where $B2=D_i\dfrac{\Gamma(2-U_2)(\Delta t)^{U_2}}{2h^{V_2}}$.

Similarly, by employing the L1 formula for time dimension and the CN method with Grunwald approach for spatial dimension in equation (45) as follows,

$$\bar{A}3\bar{\beta}^{j+1}=\bar{M}3\bar{\beta}^{j}+\left(b3_1\beta_i^{j-1}-\sum_{k=2}^{j}b3_k(\beta_i^{j+1-k}-\beta_i^{j-k})\right)+\Gamma(2-U_3)(\Delta t)^{U_3}d3(C_i^j,\,P_i^j,\,\beta_i^j)+\Gamma(2-U_3)(\Delta t)^{U_3}\bar{F}3^{j+1}. \tag{58}$$

The coefficients matrix is expressed by $\bar{A}3=[A3_{i,j}]$ for $i, j=1, 2, 3,\ldots, K-1$ as follows,

$$A3_{i,j}=\begin{Bmatrix}0 & \text{When } j\geqslant i+2\\ -g3_0B3 & \text{When } j=i+1\\ b3_0-g3_1B3 & \text{When } j=i\\ -g3_2B3 & \text{When } j=i-1\\ -g3_{i-j+1}B3 & \text{When } j\leqslant i-1\end{Bmatrix}, \tag{59}$$

where $B3=D_{\mathrm{DA}}\dfrac{\Gamma(2-U_3)(\Delta t)^{U_3}}{2h^{V_3}}$.

Consider λ_1 is an eigenvalue of $A1$, such that $\underline{A1}X = \lambda_1 X$ for some non-zero vector X. Let $|x_i| = \max\{|x_j|: j = 0, 1, 2, ...,K\}$, then $\sum_{j=0}^{K} A1_{i,j}x_j = \lambda_1 x_i$, this implies

$$\lambda_1 = A1_{i,i} + \sum_{j=0,j\neq i}^{K} A1_{i,j}\frac{x_j}{x_i}. \tag{60}$$

Putting the $A_{i,j}$ values in equation (60),

$$\lambda_1 - b1_0 - B1g1_1 - B1g1_0\frac{x_{i+1}}{x_i} - B1g1_2\frac{x_{i-1}}{x_i} - B1\left(\sum_{j=0}^{i-2} g1_{i-j+1}\frac{x_j}{x_i}\right), \tag{61}$$

$$\lambda_1 = b1_0 - B1\left(g1_1 + \sum_{j=0,j\neq i}^{i+1} g1_{i-j+1}\frac{x_j}{x_i}\right). \tag{62}$$

Since, $(\sum_{K=0}^{\infty} g1_K = 0)$ and $g1_1$ is the sole element in the Grunwald weights sequence that possesses a negative value, and $g1_1 = -V_1$ and thus for $1 < V_1 \leqslant 2$

$$-g1_1 \geqslant \sum_{K=0,K\neq 1}^{j} g1_K \text{ for } j = 0, 1, 2, ... \tag{63}$$

Since $\left|\frac{x_j}{x_i}\right| \leqslant 1$ and $g1_j \geqslant 0$, for $j = 0, 2, 3, ...,$

$$\sum_{j=0,j\neq i}^{i+1} g1_{i-j+1}\left|\frac{x_j}{x_i}\right| \leqslant \sum_{j=0,j\neq i}^{i+1} g1_{i-j+1} \leqslant g1_1, \tag{64}$$

$$g1_1 + \sum_{j=0,j\neq i}^{i+1} g1_{i-j+1}\left|\frac{x_j}{x_i}\right| \leqslant 0. \tag{65}$$

Similarly, when considering the matrix $A2$,

$$g2_1 + \sum_{j=0,j\neq i}^{i+1} g2_{i-j+1}\left|\frac{x_j}{x_i}\right| \leqslant 0. \tag{66}$$

Similarly, when considering the matrix $A3$,

$$g3_1 + \sum_{j=0,j\neq i}^{i+1} g3_{i-j+1}\left|\frac{x_j}{x_i}\right| \leqslant 0. \tag{67}$$

For interacting Ca^{2+}, IP_3 and DA systems, the matrix representation is obtained in the following manner,

$$[A]_{3K+1\times 3K+1} = \begin{bmatrix} [A1]_{K\times K} & 0 & 0 \\ 0 & [A2]_{K\times K} & 0 \\ 0 & 0 & [A3]_{K\times K} \end{bmatrix}_{3K+1\times 3K+1}. \tag{68}$$

Given that $B1$, $B2$, and $B3$ represent non-negative real numbers, all eigenvalues of $A1$, $A2$, $A3$, and A satisfy the criterion $|\lambda| \geqslant 1$. Matrix A is considered to be invertible, and it is observed that every eigenvalue of the inverse matrix A^{-1} meets a condition $|\eta| \leqslant 1$. Hence, it can be concluded that the spectral radius of the matrix $\rho(A^{-1}) \leqslant 1$, which implies that the used scheme exhibits unconditional stability.

References

[1] Palop J J, Jones B, Kekonius L, Chin J, Yu G Q, Raber J, Masliah E and Mucke L 2003 Neuronal depletion of calcium-dependent proteins in the dentate gyrus is tightly linked to Alzheimer's disease-related cognitive deficits *Proc. Natl. Acad. Sci. USA* **100** 9572–7

[2] Tu H, Nelson O, Bezprozvanny A, Wang Z, Lee S F, Hao Y H, Serneels L, De Strooper B, Yu G and Bezprozvanny I 2006 Presenilins form ER Ca^{2+} leak channels, a function disrupted by familial Alzheimer's disease-linked mutations *Cell* **126** 981–93

[3] Berridge M J 2010 Calcium hypothesis of Alzheimer's disease *Pflugers Arch. Eur. J. Physiol.* **459** 441–9

[4] Binder E, Kinkead B, Owens M and Nemeroff C B 2001 Neurotensin and dopamine interactions *Pharmacol. Rev.* **53** 453–86

[5] Stokes A H, Hastings T G and Vrana K E 1999 Cytotoxic and genotoxic potential of dopamine *J. Neurosci. Res.* **55** 659–65

[6] Qi Z, Miller G W and Voit E O 2012 Mathematical models of dopamine metabolism in Parkinson's disease *Systems Biology of Parkinson's Disease* (Springer) 151–71

[7] Bootman M D and Berridge M J 1995 The elemental principles of calcium signaling *Cell* **83** 675–8

[8] Verkhratsky A 2002 The endoplasmic reticulum and neuronal calcium signalling *Cell Calcium* **32** 393–404

[9] Wagner J and Keizer J 1994 Effects of rapid buffers on Ca^{2+} diffusion and Ca^{2+} oscillations *Biophys. J.* **67** 447–56

[10] Ahmed Z and Connor J A 1988 Calcium regulation by and buffer capacity of molluscan neurons during calcium transients *Cell Calcium* **9** 57–69

[11] Tewari S G and Pardasani K R 2010 Finite element model to study two dimensional unsteady state cytosolic calcium diffusion in presence of excess buffers *IAENG Int. J. Appl. Math.* **40** 1–5

[12] Tewari S G and Pardasani K R 2012 Modeling effect of sodium pump on calcium oscillations in neuron cells *J. Multiscale Model.* **04** 1250010

[13] Tripathi A and Adlakha N 2011 Closed form solution to problem of calcium diffusion in cylindrical shaped neuron cell *World Acad. Sci. Eng. Technol.* **80** 739–42

[14] Jha A and Adlakha N 2014 Analytical solution of two dimensional unsteady state problem of calcium diffusion in a neuron cell *J. Med. Imaging Heal. Inform.* **4** 547–53

[15] Pawar A and Pardasani K R 2022 Simulation of disturbances in interdependent calcium and β-amyloid dynamics in the nerve cell *Eur. Phys. J. Plus* 2022 1378 **137** 1–23

[16] Pawar A and Pardasani K R 2022 Study of disorders in regulatory spatiotemporal neurodynamics of calcium and nitric oxide *Cogn. Neurodyn.* **17** 1661–82

[17] Jha B K, Adlakha N and Mehta M N 2013 Two-dimensional finite element model to study calcium distribution in astrocytes in presence of VGCC and excess buffer *Int. J. Model. Simulation, Sci. Comput.* **4** 1250030

[18] Jha B K, Adlakha N and Mehta M N 2014 Two-dimensional finite element model to study calcium distribution in astrocytes in presence of excess buffer *Int. J. Biomath.* **7** 1–11

[19] Manhas N, Sneyd J and Pardasani K R 2014 Modelling the transition from simple to complex Ca^{2+}oscillations in pancreatic acinar cells *J. Biosci.* **39** 463–84

[20] Manhas N and Pardasani K R 2014 Modelling mechanism of calcium oscillations in pancreatic acinar cells *J. Bioenerg. Biomembr.* **46** 403–20

[21] Pathak K and Adlakha N 2016 Finite element model to study two dimensional unsteady state calcium distribution in cardiac myocytes *Alexandria J. Med.* **52** 261–8

[22] Pathak K B and Adlakha N 2015 Finite element model to study calcium signalling in cardiac myocytes involving pump, leak and excess buffer *J. Med. Imaging Heal. Inform.* **5** 683–8
[23] Panday S and Pardasani K R 2013 Finite element model to study effect of advection diffusion and Na $^{+}/Ca^{2+}$ exchanger on Ca^{2+} distribution in oocytes *J. Med. Imaging Heal. Inform.* **3** 374–9
[24] Naik P A and Pardasani K R 2019 Three-dimensional finite element model to study effect of RyR calcium channel, ER leak and SERCA pump on calcium distribution in oocyte cell *Int. J. Comput. Methods* **16** 1–19
[25] Naik P A and Pardasani K R 2016 Finite element model to study calcium distribution in oocytes involving voltage gated Ca^{2+} channel, ryanodine receptor and buffers *Alexandria J. Med.* **52** 43–9
[26] Naik P A and Pardasani K R 2015 One dimensional finite element model to study calcium distribution in oocytes in presence of VGCC, RyR and buffers *J. Med. Imaging Heal. Inform.* **5** 471–6
[27] Naik P A and Pardasani K R 2017 Three-dimensional finite element model to study calcium distribution in oocytes *Netw. Model. Anal. Heal. Inform. Bioinforma.* **6** 1–11
[28] Kotwani M, Adlakha N and Mehta M N 2014 Finite element model to study the effect of buffers, source amplitude and source geometry on spatiooral calcium distribution in fibroblast cell *J. Med. Imaging Heal. Inform.* **4** 840–7
[29] Kothiya A B and Adlakha N 2023 Simulation of biochemical dynamics of Ca^{2+} and PLC in fibroblast cell *J. Bioenerg. Biomembr.* **55** 267–87
[30] Jagtap Y and Adlakha N 2018 Finite volume simulation of two dimensional calcium dynamics in a hepatocyte cell involving buffers and fluxes *Commun. Math. Biol. Neurosci.* **2018** 1–16
[31] Mishra V and Adlakha N 2023 Numerical simulation of calcium dynamics dependent ATP degradation, IP_3 and NADH production due to obesity in a hepatocyte cell *J. Biol. Phys.* **49** 415–42
[32] Mishra V and Adlakha N 2023 Spatio temporal interdependent calcium and buffer dynamics regulating DAG in a hepatocyte cell due to obesity *J. Bioenerg. Biomembr.* **55** 249–66
[33] Bhardwaj H and Adlakha N 2022 Radial basis function based differential quadrature approach to study reaction diffusion of Ca^{2+} in T Lymphocyte *Int. J. Comput. Methods* **20** 2250059
[34] Tewari V, Tewari S and Pardasani K R 2011 A model to study the effect of excess buffers and Na^{+} ions on Ca^{2+} diffusion in neuron cell *World Acad. Sci. Eng. Technol.* **76** 41–6
[35] Jha A and Adlakha N 2015 Two-dimensional finite element model to study unsteady state Ca^{2+} diffusion in neuron involving ER LEAK and SERCA *Int. J. Biomath.* **8** 1550002
[36] Sala F and Hernández-Cruz A 1990 Calcium diffusion modeling in a spherical neuron. Relevance of buffering properties *Biophys. J.* **57** 313–24
[37] Furuichi T and Mikoshiba K 1995 Inositol 1,4,5-trisphosphate receptor-mediated Ca' signaling in the brain *J. Neuroquem* **64** 953–60
[38] Falcke M, Huerta R, Rabinovich M I, Abarbanel H D I, Elson R C and Selverston A I 2000 Modeling observed chaotic oscillations in bursting neurons: the role of calcium dynamics and IP_3 *Biol. Cybern.* **82** 517–27
[39] Young G W D E and Keizer J 1992 A single-pool inositol 1,4,5-trisphosphate-receptor-based model for agonist-stimulated oscillations in Ca^{2+} concentration *Biophysics* **89** 9895–9
[40] Li Y X and Rinzel J 1994 Equations for $InsP_3$ receptor-mediated $[Ca^{2+}]_i$ oscillations derived from a detailed kinetic model: a Hodgkin–Huxley like formalism *J. Theor. Biol.* **166** 461–73
[41] Allbritton N L, Meyer T and Stryer L 1992 Range of messenger action of calcium ion and inositol 1,4,5-trisphosphate *Science* **258** 1812–5
[42] Wagner J, Fall C F, Hong F, Sims C E, Allbritton N L, Fontanilla R A, Moraru I I, Loew L M and Nuccitelli R 2004 A wave of IP_3 production accompanies the fertilization Ca^{2+} wave in the egg of the frog, Xenopus laevis: theoretical and experimental support *Cell Calcium* **35** 433–47
[43] Singh N and Adlakha N 2019 A mathematical model for interdependent calcium and inositol 1,4,5-trisphosphate in cardiac myocyte *Netw. Model. Anal. Heal. Inform. Bioinforma.* **8** 18
[44] Singh N and Adlakha N 2019 Nonlinear dynamic modeling of two-dimensional interdependent calcium and inositol 1,4,5-trisphosphate in cardiac myocyte *Math. Biol. Bioinforma.* **14** 290–305
[45] Jagtap Y and Adlakha N 2023 Numerical model of hepatic glycogen phosphorylase regulation by nonlinear interdependent dynamics of calcium and IP_3 *Eur. Phys. J. Plus* **138** 399
[46] Vaishali and Adlakha N 2023 Disturbances in system dynamics of Ca^{2+} and IP_3 perturbing insulin secretion in a pancreatic β-cell due to type-2 diabetes *J. Bioenerg. Biomembr.* **55** 151–67
[47] Kothiya A B and Adlakha N 2023 Cellular nitric oxide synthesis is affected by disorders in the interdependent Ca^{2+} and IP_3 dynamics during cystic fibrosis disease *J. Biol. Phys.* **49** 133–58
[48] Kothiya A and Adlakha N 2023 Impact of Interdependent Ca^{2+} and IP_3 dynamics on ATP regulation in a fibroblast model *Cell Biochem. Biophys.* **81** 795–811
[49] Bhardwaj H and Adlakha N 2024 Model to study interdependent calcium and IP_3 distribution regulating NFAT production in T Lymphocyte *J. Mech. Med. Biol.* **24** 2350055
[50] Pawar A and Pardasani K R 2022 Effects of disorders in interdependent calcium and IP_3 dynamics on nitric oxide production in a neuron cell *Eur. Phys. J. Plus* **137** 543
[51] Pawar A and Pardasani K R 2022 Effect of disturbances in neuronal calcium and IP_3 dynamics on β-amyloid production and degradation *Cogn. Neurodyn.* **17** 239–56
[52] Pawar A and Pardasani K R 2023 Mechanistic insights of neuronal calcium and IP_3 signaling system regulating ATP release during ischemia in progression of Alzheimer's disease *Eur. Biophys. J.* (https://doi.org/10.1007/s00249-023-01660-1)
[53] Soden M E, Jones G L, Sanford C A, Chung A S, Güler A D, Chavkin C, Luján R and Zweifel L S 2013 Disruption of dopamine neuron activity pattern regulation through selective expression of a human KCNN3 mutation *Neuron* **80** 997–1009
[54] Mosharov E V, Larsen K E, Kanter E, Phillips K A, Wilson K, Schmitz Y, Krantz D E, Kobayashi K, Edwards R H and Sulzer D 2009 Article interplay between cytosolic dopamine, calcium, and α-synuclein causes selective death of substantia nigra neurons *Neuron* **62** 218–29
[55] Yamada T, Mcgeer P L, Baimbridge K G and Mcgeer E G 1990 Relative sparing in Parkinson's disease of substantia nigra dopamine neurons containing calbindin-D2sK *Brain Res.* **526** 303–7
[56] Mcmahon A, Wong B S, Iacopino A M, Ng M C, Chi S and German D C 1998 Calbindin-D 28k buffers intracellular calcium and promotes resistance to degeneration in PC12 cells *Brain Res. Mol. Brain Res.* **54** 56–63
[57] Pawar A and Pardasani K R 2023 Computational model of calcium dynamics-dependent dopamine regulation and dysregulation in a dopaminergic neuron cell *Eur. Phys. J. Plus* **123** 1–19
[58] Magin R L 2010 Fractional calculus models of complex dynamics in biological tissues *Comput. Math. with Appl.* **59** 1586–93

[59] Meerschaert M M and Tadjeran C 2004 Finite difference approximations for fractional advection-dispersion flow equations *J. Comput. Appl. Math.* **172** 65–77
[60] Du M, Wang Z and Hu H 2013 Measuring memory with the order of fractional derivative *Sci. Rep.* **3** 3431
[61] Cardoso L C, Dos Santos F L P and Camargo R F 2018 Analysis of fractional-order models for hepatitis B *Comput. Appl. Math.* **37** 4570–86
[62] Naik P A, Yeolekar B M, Qureshi S, Yeolekar M and Madzvamuse A 2024 Modeling and analysis of the fractional-order epidemic model to investigate mutual influence in HIV/HCV co-infection *Nonlinear Dyn.* **112** 11679–710
[63] Joshi H and Jha B K 2021 On a reaction–diffusion model for calcium dynamics in neurons with Mittag–Leffler memory *Eur. Phys. J. Plus* **136** 623
[64] Joshi H and Jha B K 2022 2D dynamic analysis of the disturbances in the calcium neuronal model and its implications in neurodegenerative disease *Cogn. Neurodyn.* **17** 1637–48
[65] Ezzat M A and Karamany A S E 2011 Fractional order heat conduction law in magneto-thermoelasticity involving two temperatures *Z. Angew. Math. Phys.* **62** 937–52
[66] Sousa E 2009 Finite difference approximations for a fractional advection diffusion problem *J. Comput. Phys.* **228** 4038–54
[67] Pawar A and Pardasani K R 2023 Fractional-order reaction—diffusion model to study the dysregulatory impacts of superdiffusion and memory on neuronal calcium and IP_3 dynamics *Eur. Phys. J. Plus* **138** 780
[68] Pawar A and Pardasani K R 2023 Fractional order interdependent nonlinear chaotic spatiotemporal calcium and $A\beta$ dynamics in a neuron cell *Phys. Scr.* **98** 085206
[69] Pawar A and Pardasani K R 2024 Nonlinear system dynamics of calcium and nitric oxide due to cell memory and superdiffusion in neurons *Commun. Theor. Phys.* **76** 055002
[70] Pawar A and Pardasani K R 2024 Simulation of nonlinear system dynamics of calcium and dopamine signaling *Eur. Phys. J. Plus* **139** 390
[71] Pawar A and Pardasani K R 2024 Interactive fractional-order system dynamics of calcium, IP_3 and β-amyloid in neurons *Eur. Phys. J. Plus* **139** 677
[72] Sims C E and Allbrittont N L 1998 Metabolism of inositol 1,4,5-trisphosphate and inositol 1,3,4,5- tetrakisphosphate by the oocytes of Xenopus laevis *J. Biol. Chem.* **273** 4052–8
[73] Bugrim A, Fontanilla R, Eutenier B B, Keizer J and Nuccitelli R 2003 Sperm initiate a Ca^{2+} wave in frog eggs that is more similar to Ca^{2+} waves initiated by IP_3 than by Ca^{2+} *Biophys. J.* **84** 1580–90
[74] Tello-Bravo D 1967 A mathematical model of dopamine neurotransmission *Gastron. Ecuatoriana y Tur. local.* **1** 5–24
[75] Smith G D 1996 Analytical steady-state solution to the rapid buffering approximation near an open Ca^{2+} channel *Biophys. J.* **71** 3064–72
[76] Brown S A, Morgan F, Watras J and Loew L M 2008 Analysis of phosphatidylinositol-4,5-bisphosphate signaling in cerebellar Purkinje spines *Biophys. J.* **95** 1795–812
[77] Walters S H, Taylor I M, Shu Z and Michael A C 2014 A novel restricted diffusion model of evoked dopamine *ACS Chem. Neurosci.* **5** 776–83
[78] Tadjeran C, Meerschaert M M and Scheffler H P 2006 A second-order accurate numerical approximation for the fractional diffusion equation *J. Comput. Phys.* **213** 205–13
[79] Oldham K and Spanier J 1974 *The Fractional Calculus Theory and Applications of Differentiation and Integration to Arbitrary Order* (Academic)